NTNU – Trondheim
Norwegian University of
Science and Technology

Structural properties of Ge doped multicrystalline Silicon wafers and Solar cells

Johan Carl Åke Lilliestråle

Physics
Submission date: June 2012
Supervisor: John Walmsley, IFY
Co-supervisor: Martin Bellman, Sintef

Norwegian University of Science and Technology
Department of Physics

Contents

Acknowledgement

I am very happy to have had the opportunity to do this thesis. First of all I would like to thank my Supervisor John Walmsley for helping med TEM experiments. The time for TEM investigations was very limited by we made some work at the end.
A great thank to my Co-supervisor Martin Bellman. Martin and I have worked a lot together during this thesis and it has been a pleasure.
I would also like to tank IFE in Oslo for the opportunity to use their laboratory equipment. During this work many people have trained me to use the experimental equipment, thank you all. A special thank Birgit Karlsen for always being helpful and for her good spirit and humor.

Abstract

The efficiency of multi crystalline silicon solar cells is around 17% but the theoretical limit is 33,7 %. Impurities and dislocations are the main sources for degradation of the solar cell efficiency, especially the combination. Dislocations are also responsible for plastic deformation of materials. To improve the solar cell efficiency it is important to reduce the dislocation density in the raw material for solar cells.

The nucleation and multiplication of dislocations in wafer can be suppressed by doping it with a method called *solid solute strengthening.*
In solar cells, the minority carrier lifetime, internal quantum efficiency and the solar cell efficiency are also affected by germanium despite although it is, electrically inactive in the silicon lattice.

In this thesis I have studied how all these factors are affected by germanium with different experimental methods. The main goal is to conclude if germanium could be a cost effective dopant in future solar cell production.

1. Introduction

The incoming amount solar energy on earth provides about 8000 times the energy demand of the mankind. Due to the enormous potential of solar energy it may well become a significant contributor for clean and renewable electricity in the future. The European commission for Energy and Research has stated following goals to reach for polycrystalline feedstock in solar cells before 2030:

1. Use of less than 2g of Silicon for each Watt in solar cells (today around 5g/W)
2. The cost less than 10-15 €/ kg silicon (today around 15-25 €/ kg silicon)
3. Wafer thickness less than 100 μm (today thicker than 150 μm)

To make solar cells competitive fossil fuels and achieve the stated goals many improvements in cost and efficiency must progress.[1]

1.1 Background

The crystal structure of silicon in solar cells is far from its perfect diamond structure. Many impurities enter the silicon during the melting process and dislocations are created and reproduced during the solidification process. Dislocations and impurities create intermediate energy levels in-between the electron band gaps which reduce the minority carrier lifetime and consequently the efficiency of solar cells. Plastic deformation is also enhanced by dislocations.
In this thesis, silicon ingots have been strengthened by doping them with germanium. Differences in dislocation density, solar cell efficiency, minority carrier lifetime and internal quantum efficiency have been studied.

1.2 Organization of the thesis

This thesis is mainly divided into 5 important parts. Chapter 2 discusses the background theory and a short literature overview of previous publications. The experimental methods and performance of the experiments are described in chapter 3. Chapter 4 presents the results, discussions and in in chapter 5 are the conclusions presented and suggestions to further work presented. Attachments a, b, c and d are presented in chapter 6.

2 Background theory

2.1 Literature overview

I have mainly studied 4 publications describing germanium doped silicon. In the first publication, by A.G. Ulyashin at Sintef, the minority carrier lifetime has been investigated due to different germanium concentrations in silicon. The results in the thesis indicate strong correlations between the minority carrier lifetime and the germanium concentration as expressed in table 1[2]:

Mass percent of Germanium	As cut [μs]	Gettered [μs]
2%	15	35
3-4%	12,5	22,5
7%	1,5	2,5

Table 1
The minority carrier lifetime according to different concentrations in silicon

Previous work how the dislocation density is affected by different germanium concentrations has been investigated in NTNU by Gianmaria Minozzi. Minozzi investigated multicrystalline silicon wafers with germanium concentrations between 0-1%.
According to Minozzi, the optimum germanium concentration is 0, 0155% and higher or lower values would rather increase the dislocation density.[3]
The dislocation density and its distribution in germanium doped silicon have also been studied in a publication by Martin Bellman et al. The publication surveys how the dislocation

density and the distribution are affected by germanium concentrations of 0, 15 , 60, 100 and 4000 ppma (corresponds to 0, 0.0034, 0.0137, 0,0228 and 0.912 mass percent of germanium) in multicrystalline silicon. The publication indicates that the dislocation density in silicon can be reduced up to 50% with germanium dopant, but it didn't found an accurate relationship between the dislocation density reduction and the germanium concentration.[4]
The last publication I studied was by Daren Yang et al which discuss how the material hardness, solar cell efficiency and light induced degradation in silicon solar cells are affected by germanium concentration in czochralski silicon. The publication investigates a germanium concentration of 7, $5 \cdot 10^{19}/cm^3$10, equal to 0.34 mass percent, and the results are very interesting. The most important results in the publication are:

- The fracture strength increases significantly in germanium doped wafers which reduces the breakage rate of silicon wafers in solar cell production. The breakage rates were reduced with 1% in both the solar cell fabrication process as well as in the module assembly process and around 0,5% during the cutting process.
- The solar cell efficiencies are on the same level for both the reference and the Ge-Si solar cells. But the germanium concentration seems to suppress the light induced degradation which implies that the Ge-Si cells have better efficiency in the long term and the average power output was slightly higher for the Ge-Si solar cells[5].

2.2 Crystallization of mc-Si

The Bridgman method is most used for production of multi crystalline silicon ingots and it was invented by Percy Williams Bridgman (Noble prize winner in physics in 1946).[6] In the Bridgman furnace, a silicon nitride coated crucible is gradually moved form a hot to a cold region to provide a temperature gradient for planar crystal solidification. The solidification process starts upwards from the bottom when the heat in the silicon melt is slowly removed by a heat sink.

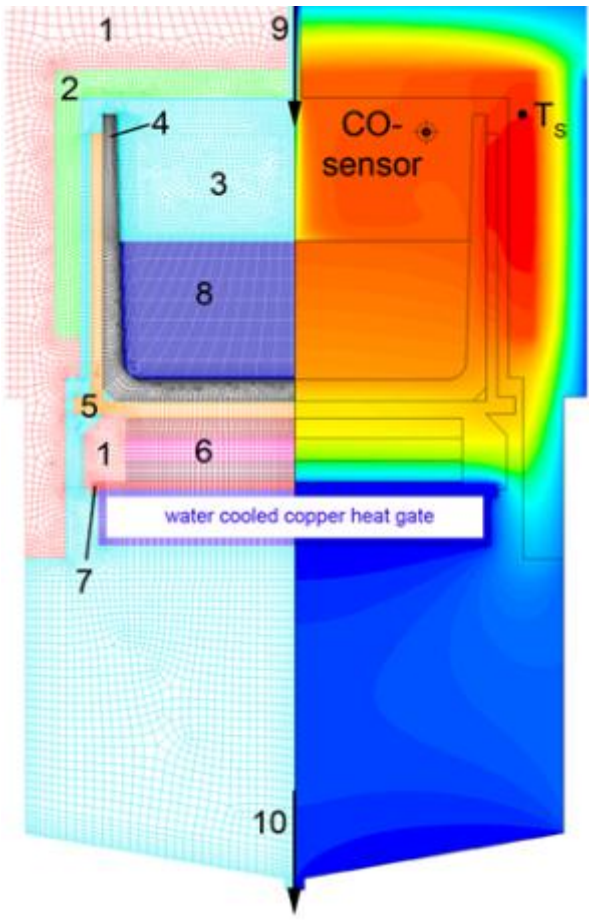

Figure 1
The most important parts of the furnace are
1)insulation, 2)susceptor, 3)argon, 4)silica crucible, 5)graphite support, 6)heat gate shutter, 7)water cooled copper heat gate, 8)silicon melt, 9)argon inlet, 10)argon outlet

The crystal growth rate in the Bridgman method depends on the temperature gradient between the solid and the melt according to the equation:[7]

Eq 1) $D_s \cdot G_s - D_L \cdot G_L = \rho_S \cdot H \cdot R$

$H = Heat\ of\ \ fusion$
$R = Growth\ velocity$
$\rho_s = density\ of\ \ solid\ metal$
$G_L = Intermediate\ temperature\ gradient\ in\ liquid\ between\ the\ solid\ liquid\ layer$
$G_s = Intermediate\ temperature\ gradient\ in\ solid\ between\ the\ solid\ liquid\ layer$
$D_L = Thermal\ conductuvity\ of\ \ liquid\ metal$
$D_S = Thermal\ conductuvity\ of\ \ solid\ metal$

Pure silicon has the crystal structure of the diamond lattice; with eight atoms in each unit cell and a lattice parameter of 5.43 Å and indirect band gaps.

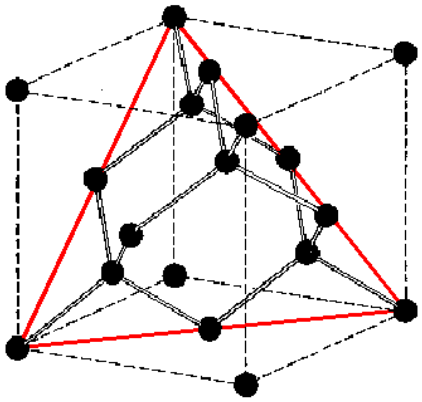

Figure 2

The diamond lattice structure

But the crystal lattice can also be viewed in the [1,1,1] direction as two interpenetrating face centered cubic lattices shifted, by ¼ of the lattice parameter with each atom surrounded by the four nearest neighbors[8].

During the solidification process, atoms in liquid phase are arrayed in positions on the surface which offers the highest coordination number (most neighbor atoms) hence it is most energetically beneficial.[9]

The silicon crystal can therefore be grown in two different ways, *"the two dimensional nucleation"* and the *"screw growth"*[*].

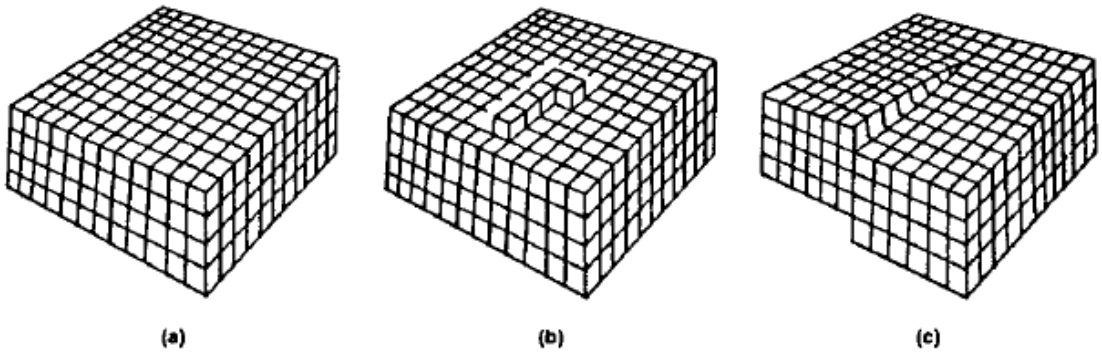

Figure 3

The screw dislocation growth in (c) demands a lower temperature gradient than the two dimensional growth in (a) and (b) because there are always free sites with high coordination number available.

In the two dimensional nucleation processes atoms are bonded onto a defect free surface and the crystal lattice is raised layer upon layer as illustrated in figure 3 a) and b).[10]

The screw dislocation growth mechanism occurs when a screw dislocation is present in the crystal lattice. The liquid atoms are then bonded to the edges of the screw dislocation, leading to spiral growth as shown in figure 3 c).

The two dimensional growth grows at a temperature gradient of 3,7 – 9 ^{0}C ^oC between the solid and liquid interfaces while the screw dislocation growth only needs a temperature gradient around 0,32-0,8 ^oC[11].

[*] See below about Screw dislocations

2.3 Defects in crystalline Si

As mentioned above crystal lattices are composed of repeating loops of ordered layers and the number of different layers is called the stacking sequence.
Any inequality of the perfect stacking sequence is considered to be a defect. The most common defects in the crystal structure are point defects, dislocations, twins, precipitations and grain boundaries. [12]

Point defects

Point defects include self-interstitial atoms, vacancies, interstitial and substitutional impurity atoms. Self-interstitial atoms and vacancies are always more or less present because of thermal vibrations in the crystal lattice. Impurity atoms can either be present as substitutional (replacing a host atom) if the radius does not differ more than 15% of the host atoms, in other cases it will occupy an interstitial sites (in between host atoms). Precipitation clusters of impurities are created if the concentration of impurity atoms exceeds its limit of solubility.[13]

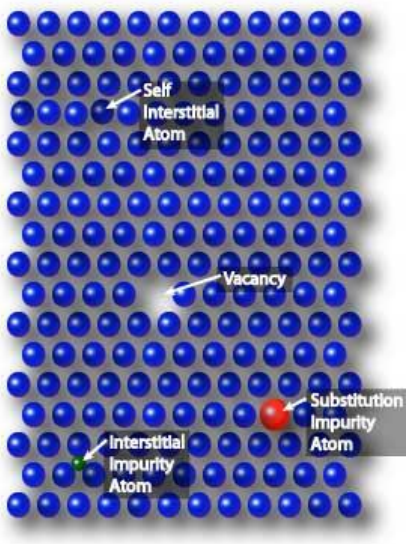

Figure 4

Illustration of vacancy, substitutional, interstitial and self-interstitial point defects in a face centered cubic lattice.

Grain boundaries

Grain boundaries are internal interfaces that separate neighboring crystal sites with different orientations. Grain boundaries reduce the electrical conductivity and the minority carrier

lifetime and starting point for corrosion for metals in general. Crystals including grain boundaries are called multicrystalline and those without monocrystalline. Monocrystalline silicon is used for electronic applications and for the most efficient Silicon solar cell applications but also more expensive and demanding to produce.[14]
The best solar cells made of mono-crystalline solar cells have an efficiency of 27,6% and 20.4% for Multi-crystalline.[15]

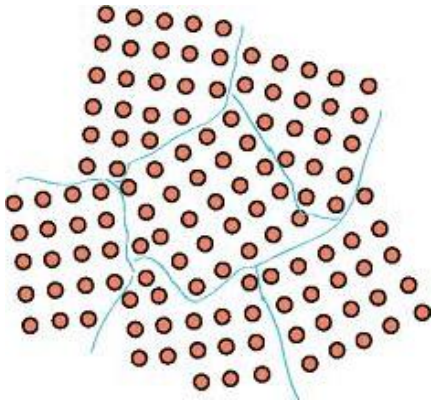

Fig 5

Illustration of Grain boundaries (blue lines)

Grain boundaries can both support and suppress dislocations propagation. According to the Hall- Petch relationship, grain boundaries act as a barrier which halt dislocations from further propagation and therefore increase the yield strength of materials, but this effect becomes counterproductive if the amount of grain boundaries exceeds a certain level[16].
Many results also indicate that grain boundaries emit dislocations during the solidification process through the so called Frank-Read multiplication mechanism and be a major contributor to the dislocation density[17].

Crystal Twinning

Twinning is a deformation when the crystal orientation changes in a lattice; it occurs if the crystal is exposed for a homogenous shear stress. The twinning implies that the stacking sequence changes in order. For example, in the [1,1,1] direction in silicon, the stacking sequence is …ABCABC… but after a twinning deformation could the stacking sequence be …ABCACB… which implies a angle between two different crystal orientations. The intermediate line that distinguishes two crystal twins is called the *twin boundary* and many twins assembled in a huge number are called *multiple twins*[18].

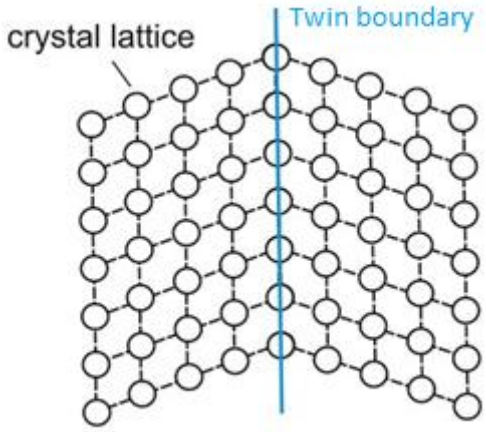

Figure 6

A twinned crystal lattice with a blue twin boundary

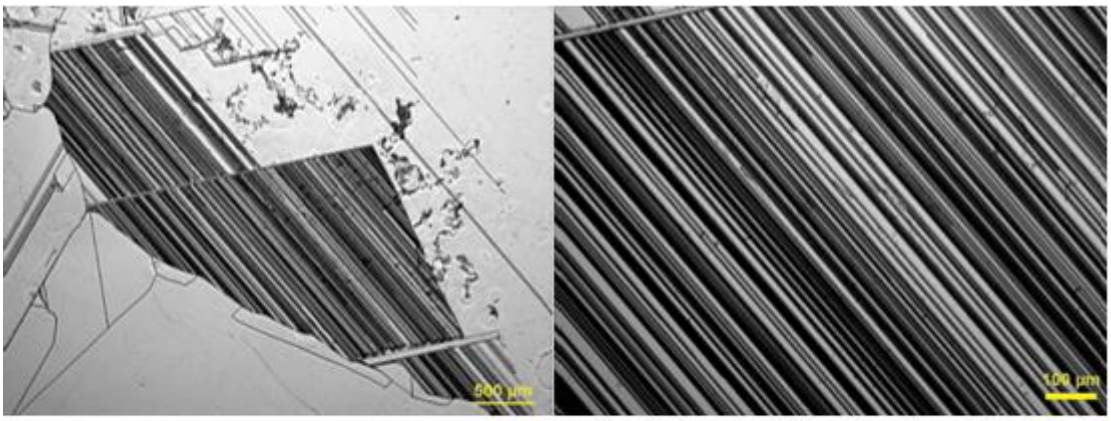

Fig 7

Images of the red twinned area in GHS1-41 picture in attachment a) taken by optical microscopy. The images illustrate multiple twins.

Dislocations

Since the birth of smelting and forging of metals, plastic deformations and brittleness have been a problem for smiths and developments have been made by trial and error experiments. In later times it was a mystery why plastic deformations occurred at shear stress values much lower than estimated from theoretical calculations. An explanation of plastic deformation was

not offered until 1934 when Taylor, Orowan and Polyani suggested that dislocations make it possible, which was experimentally verified in the 1950s. Although it was a very big advance for material science and technology nobody has received the Nobel Prize for research of dislocations[19].
The reason why dislocations enhance deformation in materials at much lower shear stresses is because they propagate on certain planes, called "*slip planes*", where only a small fraction of the bonds must be broken for propagation compared to a perfect crystal lattice.

The most important dislocations are edge and screw dislocations but they are often blended together to a more complicated structure called "mixed dislocations".
Dislocations are mainly produced during the solidification process in silicon ingots. Temperature differences in the ingot create thermal stresses which results in dislocations. To reduce the amount of dislocations it is important to keep the thermal stresses as low as possible during the solidification and cooling processes, by making the temperature gradient as smooth as possible[20].

Edge dislocations are created if an extra half plane is added or removed interstitially in between the ordinary atomic planes and a screw dislocation can be viewed as if the crystal has been cut and rejoined to accommodate a unit shear along the dislocation line (see figure 8). Dislocations are mainly characterized by three different vectors and one plane as:

1. The *Burgers vector* **b** which is defined as the opposite vector necessary to restore a crystal lattice from a dislocation imperfection.
2. The *dislocation line vector* ***t*** which describes the direction of the extra half atomic plane that intersect the crystal structure.
3. Dislocations glide on a *slip plane* and propagate in the *slip direction*, which are defined as the most atomic dense plane/direction in the crystal structure. This condition is logical because the distance between slip planes are longer than any other distances between planes which minimize the amount of shear stress necessary for the dislocation to propagate.

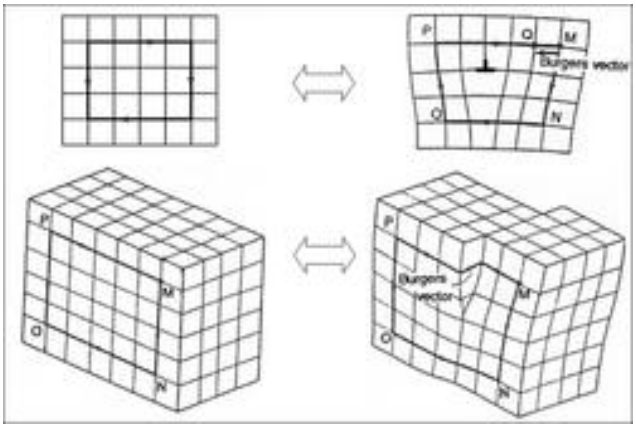

Figure 8

The upper and lower figures illustrates a edge and a screw dislocation in comparision to their perfect lattice. Real dislocations can obey a much more complicated structure and these figures are only simplifications.

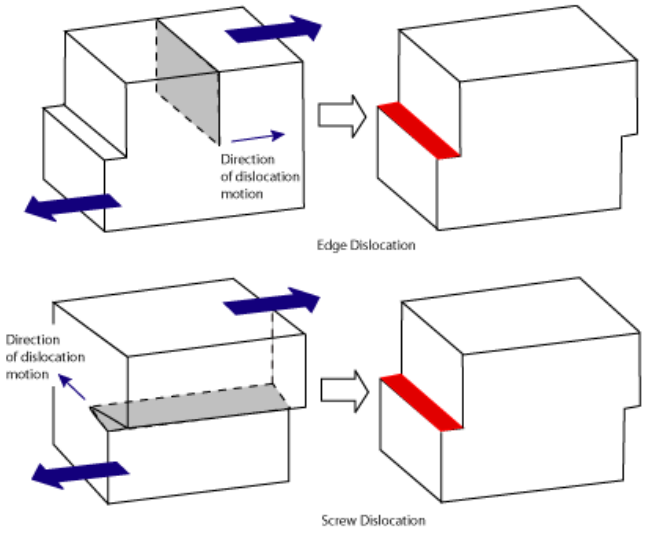

Fig 9

Note that the motions of the dislocations are parallel the burgers vector for edge dislocation but perpendicular for the screw dislocation.

Dislocations can multiply through the so called Frank Read Source (FRS) process in which dislocations are emitted from other dislocations.

Imagine a dislocation as a straight line aligned in a crystal slip plane with the two ends at A and B (see figure 10). If a force $F = \tau_1 \cdot b \cdot x$ (τ_1, b and is the shear stress, burgers vector

and x the distance between A and B), applied perpendicular to the dislocation and starts to lengthen and curve the A-B dislocation line.

If the force bends the dislocation enough it will create a full loop consisting of new dislocations. The dislocation loop can be further expanded with increasing force (τ_2 in figure 10) with the result of more dislocations. This process can be continued for many more loops and only one dislocation can give rise to many new dislocations.

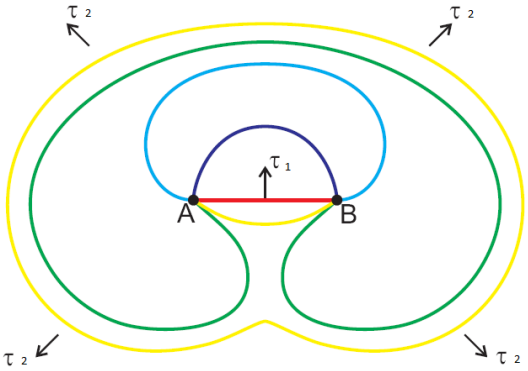

Fig 10

Illustration of the FRS process

To maintain a low the dislocation density through an ingot it is very important that the initial dislocation density in the first solidification layer is kept as low as possible to prevent further FRS reproduction.

In crystallography the parallel direction is noted $\parallel$ and perpendicular as $\top$ or $\perp$ (the longitudinal and latitudinal lines are pointing against the compressive and tensile regions of the dislocation) and the strain field around different dislocations makes them to interact. If two dislocations have the same sign of perpendicular vectors (the same direction on the stress fields) they repulse each other but if they have opposite sign they get attracted and annihilate. The different properties are summarized in table 2 below[21].

Dislocation property	Edge	Screw
Relation between dislocation line (t) and burgers vector	⊤ or ⊥	∥
Slip direction	∥ to burgers vector	∥ to burgers vector
Direction of dislocation line movement relative to b	∥	⊤ or ⊥

Table 2

Relations between the different dislocations and their dislocation lines, burgers vectors and slip directions

The density of dislocations in a crystal is defined as the total length of dislocations divided per unit volume, $\rho=l/m^3$. The range of dislocation density varies from 10^{10}-$10^{12}/m^3$ in well annealed materials and 10^{14}-$10^{15}/m^3$ in cold rolled materials.[22]

There are six possible equivalent slip planes, {001}, {110} and {111}, in the diamond crystal lattice but, only the {111} systems has been observed experimentally in Silicon.

The energy of a dislocation is proportional to the square of the length of the Burgers vector. Dislocations have therefore the shortest burger vector as possible and it is the equivalent <1,1,0> directions in silicon. This implies that the possible dislocations in silicon are {111}<1,1,0> systems. For each plane there are three possible directions of the burgers vectors. The burgers vector can be dissociated into two vectors if their conservative length does not exceed the original burger vector.

This implies that there are several different screws and mixed dislocations in silicon[23].

2.5 Impurities in Silicon

The segregation of impurities in the crystal melt can be described by the formula called Schell's equation:

Eq 2) $C_s = C_0K_{eff}(1 - f_s)^{(Keff-1)}$

C_s is the concentration of impurities in the solid
C_0 is the initial impurity concentration in the liquid
K_{eff} is the effective segregation coefficient
f_s is the mass fraction of the melt that is solidified.

The accurateness of Scheil's equation improves with slower solidification speed. Real distributions of impurities can differ much due to perturbations in the solidification process.[24] Scheil's equation can also be dependent on the impurity concentration.

Different impurities are always more or less abundant in industrial Silicon. Oxygen and Carbon are the two major impurities in silicon ingots and normal concentrations are usually between 8-40 ppm of oxygen and 0,4-8 ppm of carbon. Almost all the Oxygen and Carbon impurities are introduced during the smelting process of the raw material.
The oxygen is added through dissolved quartz from the crucible walls through the reaction $SiO_2 \rightarrow 2SiO$. It is hard to determine the segregation coefficient for oxygen in silicon because SiO evaporates from the top of the Silicon melt and many different values are found from different literatures. If the evaporation was absent the segregation coefficient would be around 0, 85 but for the ingots used in this thesis, it is estimated to be around 1,40[25].
Free oxygen atoms occupy interstitial sites between silicon atoms. Oxygen atoms normally get bonded to two neighboring silicon atoms to SiO_2 (assumed to be electrically inactive) or four bonds to SiO_4 which is electrical active and acts as a n-conduction compound in the Silicon crystal lattice. The oxygen compounds increase the rate of stacking fault formations, recombination rate and the leakage current in transistors and should therefore be avoided as much as possible[26].
Many investigations have shown that SiO_2 can precipitates and significant influence the minority carrier lifetime in solar cells. This has been observed in TEM microscopy where oxygen precipitates are mainly seen in octahedral shapes, bounded by eight equivalent $\{1,1,1\}$ planes[27].
Deep level transient spectroscopy measurements indicate that discrete energy levels between the silicon and SiO_2 precipitates interfaces are created which strongly enhance the rate of SRH recombinations[28].
The solubility of oxygen is hard to determine because the tendency for SiO_2 clusters to merge into precipitations depends very much on thermal history and annealing process of the ingot[29].
Carbon impurities are added when the evaporated SiO gas reacts with the graphite heater or other carbon containing parts in the furnace. SiO reacts with the graphite parts in the furnace, which dissociates in the melt through C and O

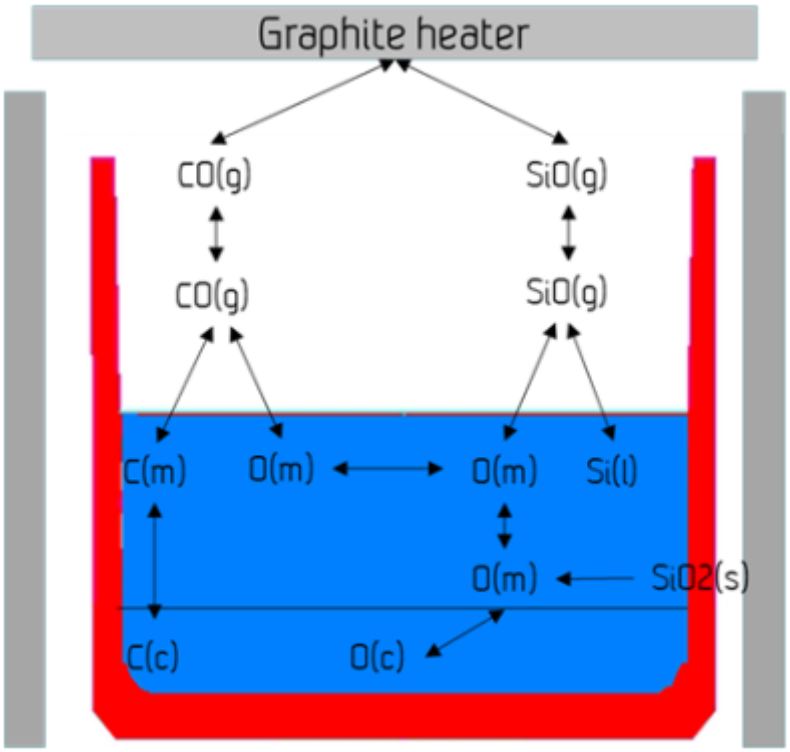

Figure 11

The carbon and oxygen cycle in a silicon melt.

Carbon impurities concentrate at the top of an ingot because the segregation coefficients in silicon is only 0,07. Substitutional Carbon atoms are not electrically active because its valence band contains only 4 electrons and they occupy substitutional lattice sites.
Anyway, carbon is an unwanted impurity because it might reduce the minority carrier lifetime, change the lattice parameter, the boron distribution in p-doped ingot and enhance the support of oxygen precipitations. The solubility level of carbon is estimated to 11 ppma in solid silicon and precipitates are considered to form Si-C bonds[30].

Different metal impurities are also present in silicon melts, especially iron and copper which mainly originate from the crucibles material.
The tolerance for metals in solar cells is very low because they reduce the minority carrier lifetime. But the segregation coefficients for different metals are in general between 10^{-2}-10^{-8} and most of them segregate towards the top of an ingot[31]. Impurities can diffuse back from the crucible walls during the cooling process as expressed in figure 12 which can be a serious problem for the sides of a silicon ingot.

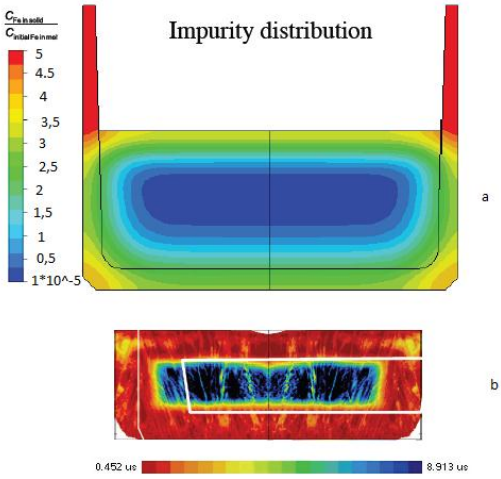

Figure 12

Figure a) shows the concentration of back diffused Iron after 25 hours of cooling. The steep reduction in the minority lifetime can partly be explained due the Iron concentration. This experiment illustrates the importance of clean crucibles.

Some impurities, like carbon, Iron and Nickel not only reduce the minority carrier lifetime but also induce structural defects which enhance the risk of shunting and short circuit in Solar cells.[32]

2.6 Solution hardening

The equation for changes in Gibbs free energy in chemical reactions is defined as:

Eq 3) $\Delta G = \Delta H - T\Delta S$

The change in entropy is very little compared to the change in enthalpy in the formation of dislocations. This implies a positive change in the Gibbs free energy when dislocations are created.

Dislocations are therefore defined as none equilibrium defects which occur only due to external difference in temperature and stress fields[33]. There are several methods to strengthen material and in this thesis is *"solid solution strengthening*", by adding germanium atom used. The solid solution strengthening increases the yield stress of materials and prevents dislocations from FRS multiplication.

Substitutional alloy atoms have a tendency to diffuse to the core of dislocations and be located at a lattice point that fits their sizes and radiate a stress field which interacts with other dislocations. The alloy atoms can be viewed as buffers which “anchor” the dislocations from further propagation.

The interaction between a substitutional atom and a dislocation is strong if it is located above, below or near the dislocation core.

For example, for an edge dislocation a smaller (compared to the host atoms) substitutional atom can diffuse into the compressive part above the dislocation core and a larger substitutional atom to the tensile part below the dislocation core and reduce out the elastic strain energy and reach the highest entropy of the system, as illustrated in figure 13. The result is a binding energy between the substitutional atoms and the dislocations.[34]

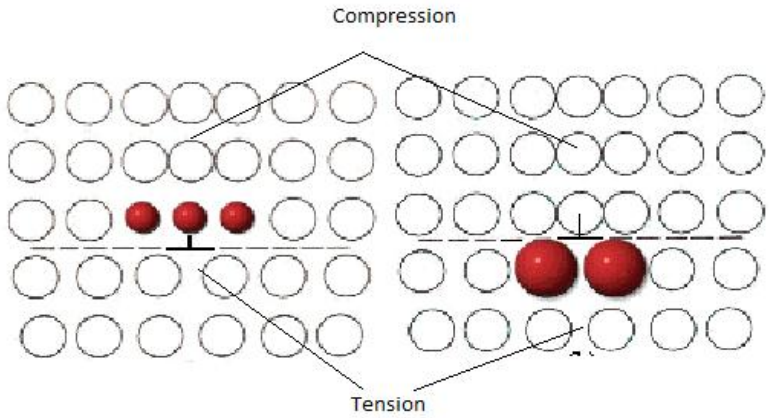

Figure 13

The figure illustrates a larger and smaller substitutional occupy a tensile and a compressive part in the lattice

The energy of a dislocation is determined by the length of the Burgers vector and the shear modulus of the material. Briefly, the change in yield strength depends on three factors, solute concentration, difference in atomic radii and shear modulus between the solute and host atoms, which is expressed in equation 4 below.

$$\Delta\tau = Gb\varepsilon^{3/2}\sqrt{c}$$

$$\varepsilon = \left|\varepsilon_a - \beta\varepsilon_G\right|$$

Eq 4) $$\varepsilon_a = \frac{\partial a}{a\partial c}$$

$$\varepsilon_G = \frac{\partial G}{G\partial c}$$

G is the shear modulus of the solvent atoms and b is the burgers vector.

The formula expresses the fact that the yield stress increases if the local lattice vector and local shear moduli change according to the derivate of the solute concentration.
The shear moduli of the solute atoms should be lesser than the solvent to obtain a strengthening of the material.
The limit of the material strengthening is dependent on the solubility of the solute and solvent atoms. If the concentration of the solute atoms exceeds the solubility limit, precipitations will be created which rather reduces the yield strength. The shear modulus and lattice parameters of Silicon and Germanium are:

Element	Shear modulus	Lattice constant
Silicon[35]	52-80Gpa	111pm
Germanium[36]	41Gpa	122pm

Table 3

Shear modulus and lattice constants for silicon and germanium

Germanium is electrically inactive in silicon and due to the differences of the lattice constant and shear modulus it is a beneficial solute in Silicon.
As mentioned earlier the dislocations consist of screws and mixed dislocations.
The interactions between the solute atoms and the screw dislocations are expected to be very small because a screw dislocation does not change the local lattice parameter. Still some interaction is expected due to the differences in local shear module but it decreases proportional to $1/r^2$.
Germanium has 10% larger atomic radius than silicon and it is therefore likely that they occupy the substitutional tensile of the mixed dislocations[37].

2.7 Minority carrier life time

The minority carrier lifetime is very important for the diffusion length of charge carriers in a solar cell. Recombination is the process when excited charge carries annihilate and the electrostatic energy is transformed to photons and/or phonons. There are mainly three types of important recombinations: radiative recombination, Shockley Read Hall recombination (SHR) and Auger recombination.
Radiative recombination occurs when excited electrons and holes spontaneously recombine. The time the charge carriers are excited before recombination is called the m*inority carrier lifetime* and is defined as:

Eq 5) $t_e = \frac{\Delta n}{R},\ t_h = \frac{\Delta p}{R}$

e stands for electrons and h for holes, Δn/Δp are the number of excited electron and holes R is the recombination rate.

Shockley-Read-Hall recombination (SRH) occurs when charge carriers recombine through intermediate band gaps. This is of great importance for elements and compounds with indirect (like silicon) band gaps because the trapped states can absorb the necessary amount of momentum which is needed for recombination. The recombination rate from the SRH recombination is defined as:

Eq 6) $t_{SRH} = \frac{t_{n0}(p_0 + N_v e^{(E_v - E_t)/kT} + \Delta n) + t_{p0}(n_0 + N_c e^{(E_t - E_c)/kT} + \Delta n)}{p_0 + n_0 + \Delta n}$

Where t_{n0} / t_{p0} are the minority and majority (depending on if the material is n or p doped) carrier lifetimes expressed as**:**

Eq 7) $t_{n0} = (N_t \cdot \sigma_n \cdot v_{th})^{-1}$
$t_{p0} = (N_t \cdot \sigma_p \cdot v_{th})^{-1}$

σ is the capture cross section for the trapped level and v_{th} ***is the thermal velocity of the charge carriers.***

It is obvious from equation 6 and 7 that the lifetime is reduced to maximum when a trapped level is located in the middle of the band gap.

The surface of a material contains often higher amount of impurities than the bulk and therefore differ their lifetimes also. The total lifetime of the surface and bulk is then defined as[38]:

Eq 8) $$\frac{1}{t} = \frac{1}{t_{bulk}} + \frac{1}{t_{surface}}$$

The formula must be adjusted in regard to how much of the light that reaches the bulk before being absorbed.

Different impurity elements can be very devastating for the minority carrier lifetime because they create intermediate band gaps. In Silicon ingots Oxygen and Carbon are the most present impurities from the solidification process but different kind metals are most disastrous for the minority carrier lifetime. Figure 14 illustrates how the efficiency is reduced in a 4 ohm cm p-base device due to different metal impurities.

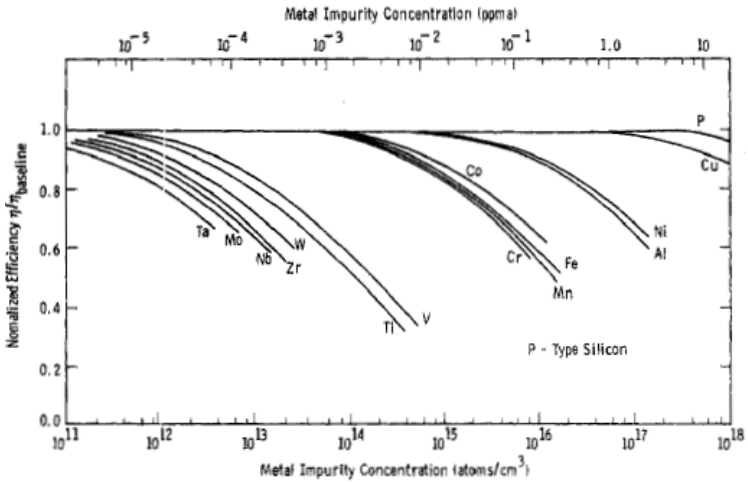

Figure 14

Measurements by A. Rohagti indicate that metal impurities can significantly affect the minority carrier lifetime even at small concentrations.

For example, it is sufficient with only 0,002ppma or iron to reduce the efficiency with 20% according to figure 14[39].

Auger recombination occurs when the resulting photon energy from a former recombination excites or ionizes another electron hole pair.

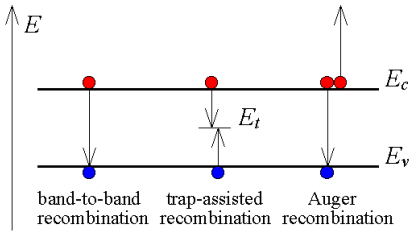

Figure 15

Briefing of the three most important recombination processes

Dislocations also reduce the minority carrier lifetime because they create intermediate bands which enhance SRH recombination. Dislocations can also interact with impurities with the result of decorated impurities. Decorated impurities reduce the minority carrier lifetime much more than single dislocations or impurities through the mechanism illustrated in figure 16[40].

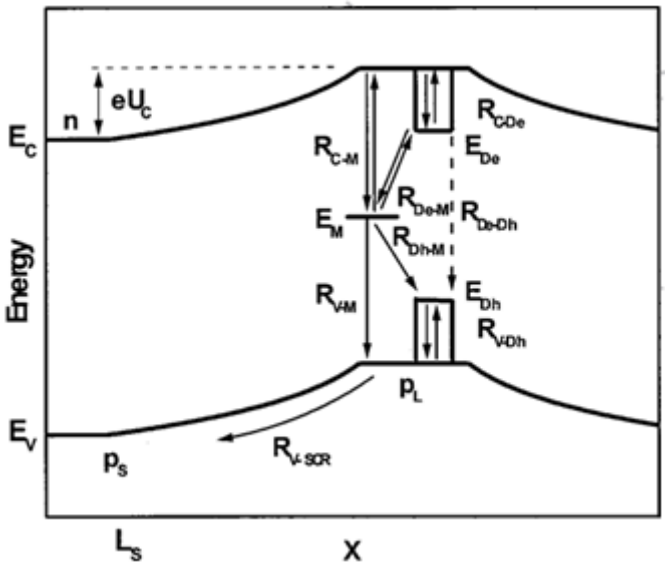

Figure 16

The initial dislocation creates the intermediate band gaps E_{Dk} and E_{De}, and the impurity atom creates another energy level at E_M. The energy levels of the valance and conduction band are raised because the dislocations have a tendency to trap excited charge carriers. Charge carriers can then easier annihilate through the smaller energy gap R_{De-M} and R_{Dk-M} compared to R_{De-Dh}

3 Experimental Methods

3.1 Ingots and wafers used in this thesis

The Silicon wafers used in this thesis were doped with germanium and named as described table 4.

Ingot	Germanium [%]
GHS1	1
GHS2	0
GHS3	0,006

Table 4

Germanium concentrations in the different ingots used in this thesis.

From the center (to avoid back diffused impurities) of each ingot a $5\times10\times10\cdot cm^3$ cuboid, cut out as illustrated in figure 17. All wafers where then cut out with a wire saw with thicknesses of 3.15 and 0.45mm and the thinner wafers were used for solar cells. Because of losses in the cutting process the real thicknesses and positions presented in attachment b. The ingots had the initial weight of 12 kg, a height of 100 mm and a radius of 125 mm. During the solidification process the growth rate was approximately 10 mm/hour and due to the slow solidification it is most likely that the ingots has been grown in the [1,1,1] direction, which is the most dense structure[41].

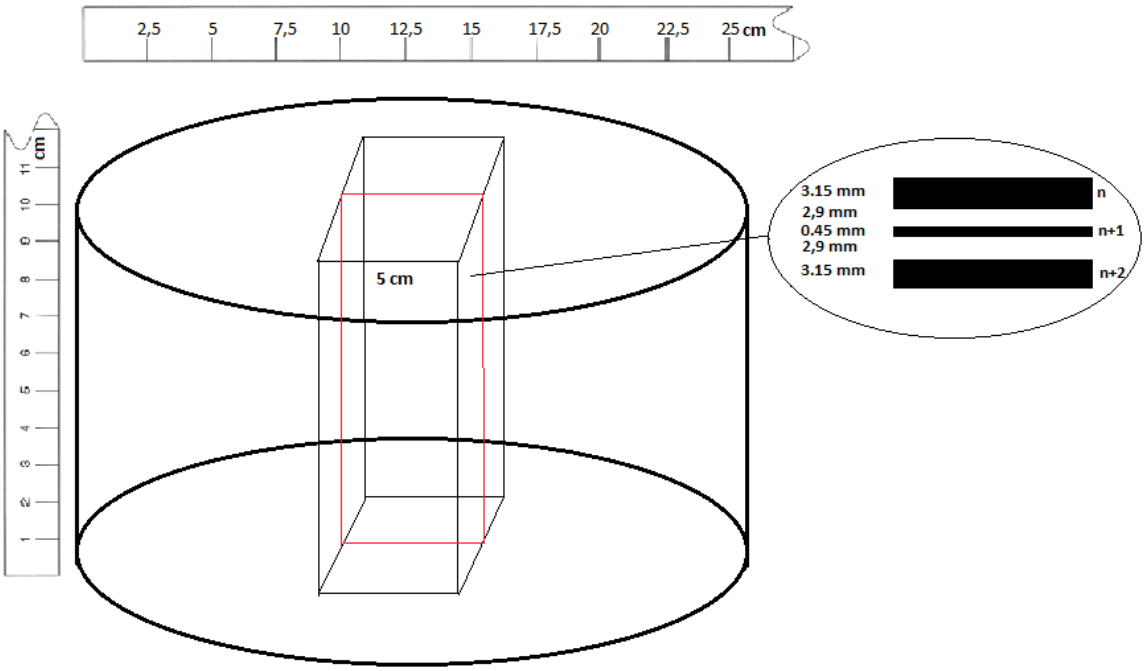

Figure 17

Illustration of the silicon ingot, the cuboid in the middle illustrates where the wafers originate from. The black strips to right illustrate a cross sections of the wire saw where n is an odd number. All thick wafers are named with odd numbers and all thin with even numbers in the thesis.

3.2 Sample preparation

An extensive sample polishing preparation is necessary to do before etching the wafers for P.V scan measurements. The wafers were polished in three steps, 3 times mechanically with the mesh sizes 300, 900 and 1200 particles/cm^2, three times with a diamond spray with particle sizes of 9, 3 and 1 µm and a final step with silica particles of 50-70 nm in diameter. The dislocations are usually too small to be detected in P.V scan and must be enlarged with an etching process. The etching process used in this thesis was:

1. RCA1 10 min
2. DI-water
3. 5% HFCa 3 min NB! 12l 5% HF (600 ml HF)
4. Sopori etching 25 sek New Sopori etching (11 sek)
5. Clean with ethanol
6. Dry in room temperature

3.3 Oxygen and Carbon measurement

Fourier Transform Infrared Spectroscopy (FTIR) is a technique used to identify organic and inorganic compounds in wafers. In FTIR, infrared light is emitted through a sample and the absorption can reveal the presence of impurities and concentrations.
The FTIR uses a beam splitter to split the infrared light into two beams. Two mirrors reconnect the light again but one of them moves back and forth which results of an interference pattern. The pattern is the Fourier transform of the infrared absorption spectroscopy which illustrates the abandon of certain impurity elements[42].

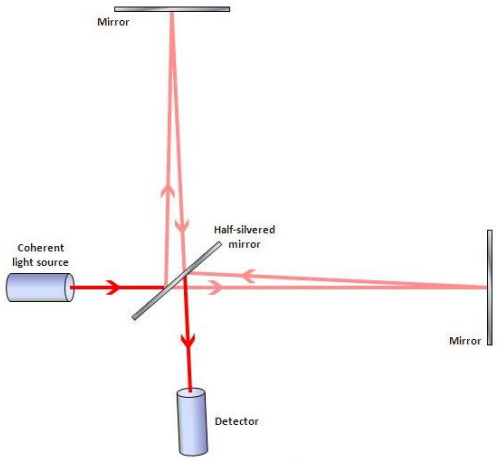

Figure 18

The interference pattern of the splitted and reconnected light is the fourier transformation of the absorption spectrum for a certain element.

In this thesis, 26 wafers from the GHS3 and 11 from each of the GHS2 and GHS1 ingots examined with FTIR to detect the oxygen and carbon concentrations. The wafers from the GHS3 ingots were examined by the author of this thesis and the GHS1 and GHS2 ingots were investigated by Martin Bellman with the wavelengths of 605 cm^{-1} and 1107 cm^{-1} for the carbon and oxygen concentrations[43].

3.4 Germanium concentrations

Electron probe analyzer (EPMA) was used to detect the Germanium concentrations in the silicon ingots. The EPMA uses highly energetic electrons to bombard a sample. If electrons from the inner shell become ionized of the electron beam it is possible that other electrons auger recombine to the inner shell. The amount of released energy from the outer electron is proportional to the atomic number Z. With the characteristic wavelengths of the re-emitted light, it is possible to survey different amount of elements in a sample. The EPMA is more accurate for elements with larger atomic numbers and the limit for germanium in silicon is estimated to 0.01% [44]. 32 wafers from the GHS3 ingot 26 wafers from each of the GHS1 and GHS2 ingot were investigated by Morten Raanes at NTNU. In the GHS1 ingot were two measurements, 35 mm and 105 mm from the center of the ingot performed.

3.5 Dislocation density measurement

Photo Voltaic scan (PV-scan) is used to measure the defect density on polished and etched wafers. A laser beam illuminates the wafer perpendicularly and the back scattered reflection is either of high or low angles, according to the size of the reflecting etch pits. Etch pits of dislocations usually appear as broad holes while grain boundaries have more V-shaped morphology.

This implies that reflected laser light from dislocations possess a high angle and a low angle from grain boundaries. An integrated sphere detects the high angled light from dislocations and a separate detector distinguishes them from the low angled scattered light.

The wafers were scanned with a resolution of 50 microns and a scan speed of 5 mm/s.

All wafers were scanned over a $50\times50mm^2$ area, but 5 mm from each edge was erased to avoid false dislocation scanning. According to observations by Gaute Stokkan, multiple twins exaggerate the dislocations density because they create interference patterns that scatter light in all directions.[45]

It is therefore very hard to make an accurate error analysis of the PV images. The error analysis in this thesis was performed by estimating the total area of multiple twins from the dislocation density with. Figure 19 is an example of how to make the error analysis:

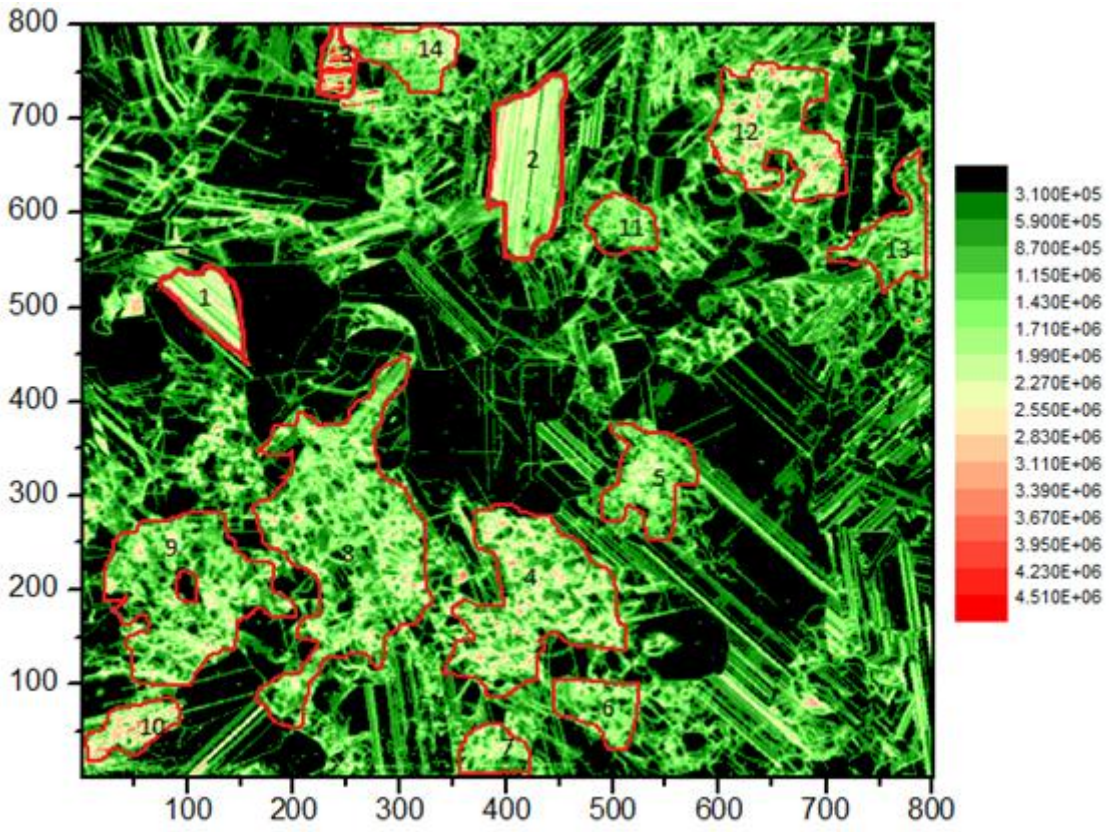

Figure 19

PV scan image of the GHS3-5 wafer. The marked areas around 1, 2and 3 are most likely to be multiple twins and the areas in number 4-14 are probably dislocation cluster. The scale bar to right indicates the number of dislocations per cm2. The X and Y scales express the scan resolution of the P.V scan which 5×10^{-6} m. The lengths of the axis are then equal to 40 mm.

1. Choose a certain dislocation density number which distinctly represents typical dislocations. All other contrasts are then black compared with the dislocations of importance. In figure 19, 3.1×10^{5} /cm^{2} has been chosen as the distinguishable dislocation density.
2. Calculate the percentile area of the total amount of the remaining visible dislocations. 61% of the area is covered with a dislocation density greater than 3.1×10^{5} /cm^{2} in figure 19. The area of dislocations was calculated in MATLAB with the code:

```
clear all
clc
a21 = Matrix;        %name on the matrix of the dislocation density
[m,n] = size(a21);
teller = 0;
summa = 0;
for i = 1:m,
    for j = 1:n;
        if(a21(i,j)>=3.1*10^5)  %Counts all dislocation spots
            teller = teller +1;
        end
    end
end

dj=(1-teller/(m*n))*100;       %Calculates the area which contain
                               %fewer dislocations than 3.1*10^5/cm^3
```

3. Mark the area of all suspicious multiple twins areas and calculate their percentile area. The areas of 1, 2 and 3 in figure 19 occupy 5% of the total area. This can be done in photo shop or in the free ware Image J.
4. Do the same procedure for areas with dislocation clusters. The dislocation clusters marked 4-14 occupies around 30% of in figure 19
5. The multiple twins and dislocation clusters that have been marked make 35% of the total image. The remaining area of dislocations must then be 61%-35% = 26%.
6. The remaining dislocations of 26% of the total image are estimated with the bare eye. I personally consider the rest of the dislocations to be 20% of dislocation cluster and 6% of twins.
7. The multiple twins are then assumed to occupy 11% of the total image. The area consisting of pure dislocation cluster is therefore 61% to 50% of the total image.

This error analysis is only a rough approximation and the certainty depends on how easy it is to distinguish dislocation clusters from multiple twins in PV scan images and how much time that can be dedicated to it.

3.6 Minority carrier lifetime measurements

Microwave Photo conductance Decay (μw-PCD) measures the minority carrier lifetime and Iron concentration in silicon wafers. The μw-PCD illuminates a sample with an infra-red laser of 904 nm which creates free electron hole pairs. The abundance of free charge carriers is then proportional to the conductivity of the sample. The decay of the conductivity can be monitored by detecting the microwave reflectivity because the power of a reflected microwave is proportional to the conductivity and measured as a function of time. The penetration depth of 904 nm laser light in silicon is around 30 μm which covers the front surface of the sample[46]. It is therefore necessary to perform the μw-PCD measurements both before and after wafers have been gettered to evaluate the differences between the bulk and surface. In this thesis the wafers were polished and etched to get them clean and ready for the gettering process. In the gettering process the wafers were first exposed to phosphorous and then heated to about 890 °C for 20 minutes. The very near edges were removed in a CP5 etching. The wafers were then again exposed for the same etching process and finally threated by a new anneal process at 450 °C. The etching process and the experiment were performed by Rune Søndenå at IFE, Oslo.

3.7 Internal quantum efficiency measurements

Light Beam Induced Current (LBIC) is used to measure the short circuit current, minority carrier diffusion length and the internal quantum efficiency, IQE of solar cells.
The LBIC measures the reflected light from a solar cell while it is illuminated with light of a certain wavelength. The IQE can then be calculated as:

$$IQE = (1 - R) \cdot \frac{I_{SC}}{\Phi_q}$$

Eq 3) $I_{SC} = Short\,circuit\,Current$

$R = Total\,resis\tan ce$

$\Phi_q = Photonflux$

The scanning is done by deflecting the beam or by moving the solar cell wafer.
In this thesis was the light induced beam experiments were performed with a wavelength of 832 nm which corresponds to the photon energy of 1.485 eV. This photon energy is far above the ionization energy of Silicon which is around 1.1 eV and therefore should all possible charge carriers be excited[47].
Three wafers each from the GHS1 and GHS2 ingots were studied with LBIC by Felix Dreckschmidt at "*TU Bergakademie Freiberg Institut fuer Expermintelle Physik*". The wafers were polished and etched and measured with following steps:

1. CP5 ets 90 sec. Removes 4-5 μm on each side
2. Cleaning in HF and Piranha-solution
3. HF-dip and passivation
4. Annealing and lifetime measurements
5. CP5 etching in 60 sec. Removes the a-Si:H-layer. The CP5 etching removes probably 1-2 μm on each side
6. P-spraying and diffusion in a "belteoven"
7. Phosphorus glass removing in HF
8. CP5-etching in 90 sec to remove emitter. Ca. 3-4 μm removes on each side.
9. Cleaning in HF and Piranha-solution
10. HF-dip and passivation
11. Annealing and lifetime measurements

3.8 Solar cell efficiency measurement

A solar simulator produces light in order to imitate real outdoor sunlight spectrum and obtain a verifiable indoor test facility in the laboratory environment. The Solar simulator is used to test efficiency and light induced degradation of solar cells, sun screen, plastics, among others.[48]

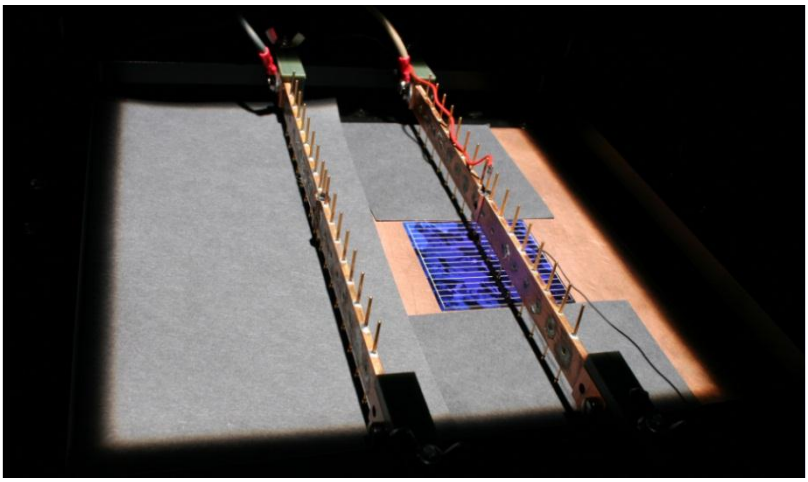

Figure 20

The most important part of the Solar Simulator used at IFE in Lillestrøm. A solar cell is placed on a copper plate around isolating papers while it is exposed for artificial sunlight. The metal pipes in the middle records the induced current, voltage and fill factor. The metal can also damage the solar cell by forcing the n and p layers into contact.

20 wafers from the GHS-1 and GHS-2 ingots and 13 from the GHS-3 ingots were manufactured into solar cells and measured in a solar simulator by Rune Søndenå at IFE, Oslo. Each wafer was produced and etched in following steps:

1. Chemically polished with CP5 solution (removes 10 of the width).
2. The n-emitter layer was created by the $POCl_3$-process in a tube furnace.
3. Anti-reflectance coating consisting of approximately 80 nm SiN_X:H was deposited in a PECVD chamber (Oxford 133, low temperature table).
4. Front and back contacts were then screen printed onto the wafers and Aluminium covers the whole backside creating a back surface field.
5. After laser edge isolation, the silver fingers and busbars on the front side were fired through the ARC.

3.9 Transmission Electron Microscopy

Transmission electron microscopy (TEM) is an electron microscope and it is the most powerful kind of microscope in the world. In TEM operation, an electron beam is focused onto a specimen and transmitted to fluorescent screen. An image is formed due to the interaction between the specimen and the electrons on the fluorescent screen.
The electron beam must obey certain condition to diffract, according to the crystal structure of the specimen. If an electron beam with wavelength λ is transmitted with the angle α normal to the crystal plane of the specimen, it subjects to Braggs law under following conditions:

Eq 10)) $n \cdot \lambda = 2 \cdot d \cdot \sin(\alpha)$

n is an integer and d is the interplanar distance.

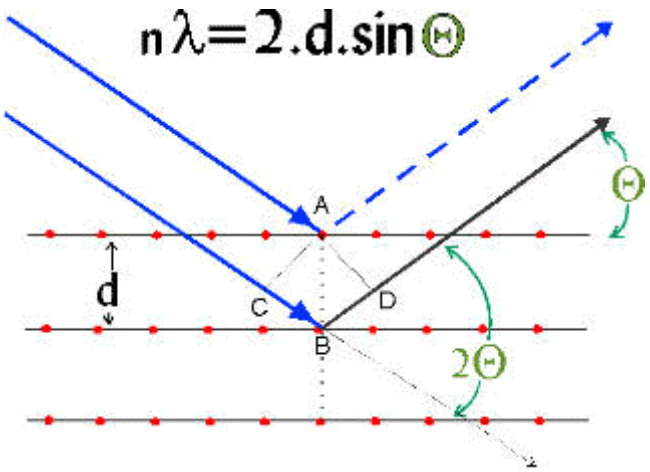

Figure 21

The Braggs law expresses the difference in path between two beams if they are reflected against two crystal planes.

The lattice spacing a, between two planes according to the miller indices' can be expressed with Braggs law as:

Eq 11) $d_{hkl} = \dfrac{a}{\left[h^2 + k^2 + l^2\right]^{\frac{1}{2}}}$

h, k and l are the miller indices and a is the lattice constant of the cubic crystal structure

The combination of equation 10 and 11 gives an expression for the incident angle of the electron beam according to the crystal direction and the wavelength as[49]:

Eq 12) $$\sin(\alpha) = \frac{n \cdot \lambda \cdot \left[h^2 + k^2 + l^2\right]^{\frac{1}{2}}}{2 \cdot a}$$

Diffraction can only occur due to some certain angles which are called the selection rules. For silicon the selection rules, when h, k and l are all odd or when they are all even in the relation h+k+l=4n[50]

TEM can also operate in the low energy electron diffraction (LEED) mode which illustrates the crystal structure in the reciprocal space. The reciprocal lattice is the Fourier lattice of the real space lattice, in other words the inverse projection of the real space lattice, which makes it possible to determine crystallographic directions of the real space image.

The sample must be very thin around the detection area to make it possible to transmit the electron beam through. The first step in the preparation process is to cut out a disc with a diameter of 3 mm from an interesting area to examine. The center of the specimen disc is then grinded until it is 20 micrometer thick by a dimpling machine. Through ion gun bombardments, a very little hole through of the remaining 20 microns is created. Just the very near areas around the hole are thin enough to be examined and it is very easy to demolish the sample during or after the sample preparation.
In this thesis it was intended to study how dislocations interact with germanium and oxygen precipitates with TEM. But due to many other experiments, delays and unsuccessful etchings of the wafers were most TEM operations aborted. John Walmsley and I decided to just detect basic defects like grain boundaries and twins as an introductory work. Due to the problems with the etching process, it was not possible to point out suspicious dislocations and precipitations with P.V scan and an optical microscope was used instead. In this thesis one sample was prepared as seen in figure 22 below.

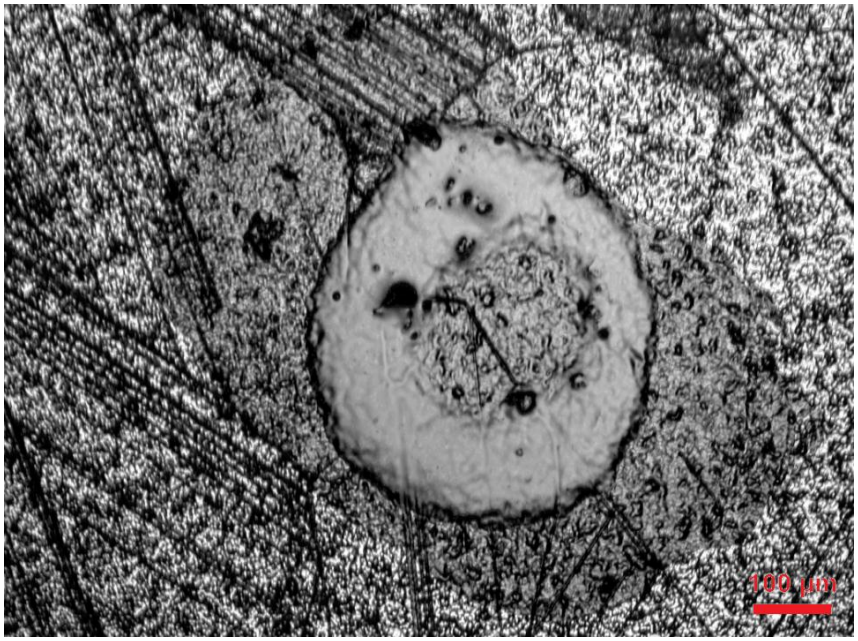

Figure 22

The figure shows an optical image of the sample used for TEM examinations. It illustrates a grain boundary which prevents multiple twins from further propagation. The ink drop in middle was used to mark the area for TEM preparation. The area was chosen with the expectation of detecting grain boundaries and twins.

4 Results and discussions

4.1 Oxygen and Carbon concentrations

All the experimental values of the carbon and oxygen concentrations are compared with their corresponding Scheil distribution.

The initial impurity concentrations C(0) in equation 2 were estimated as the average concentrations from all measurements.

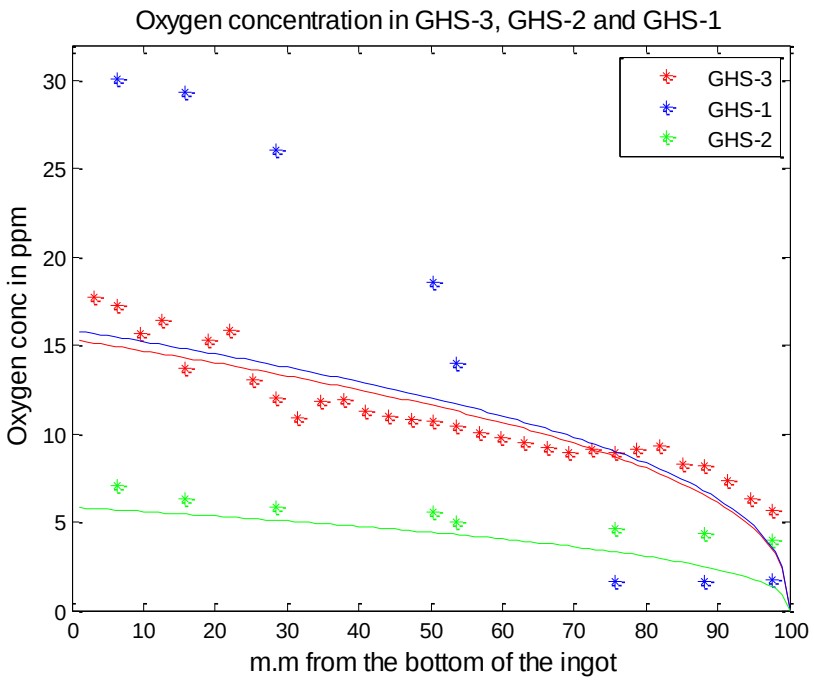

Figure 23

The doted curves are the measured values and the lined curves are the Scheil curves.

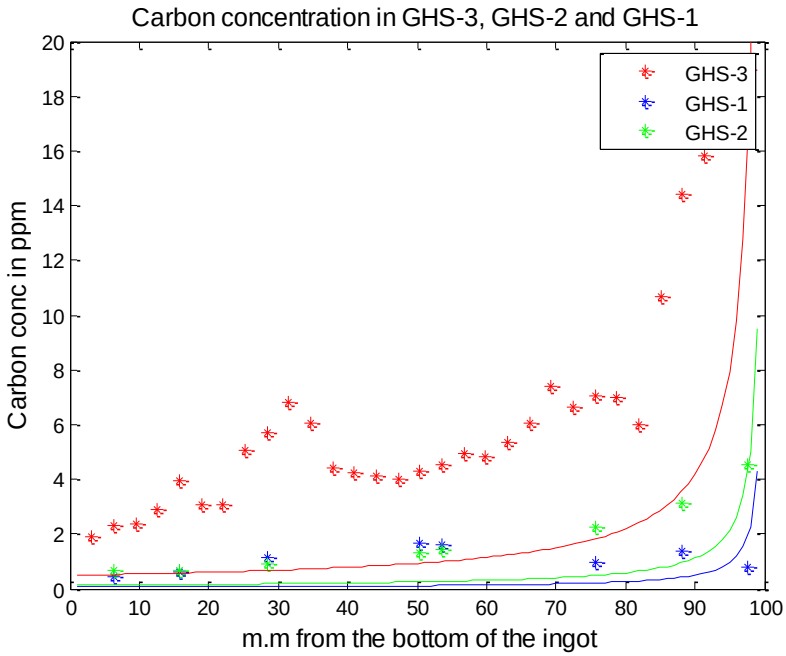

Fig 24

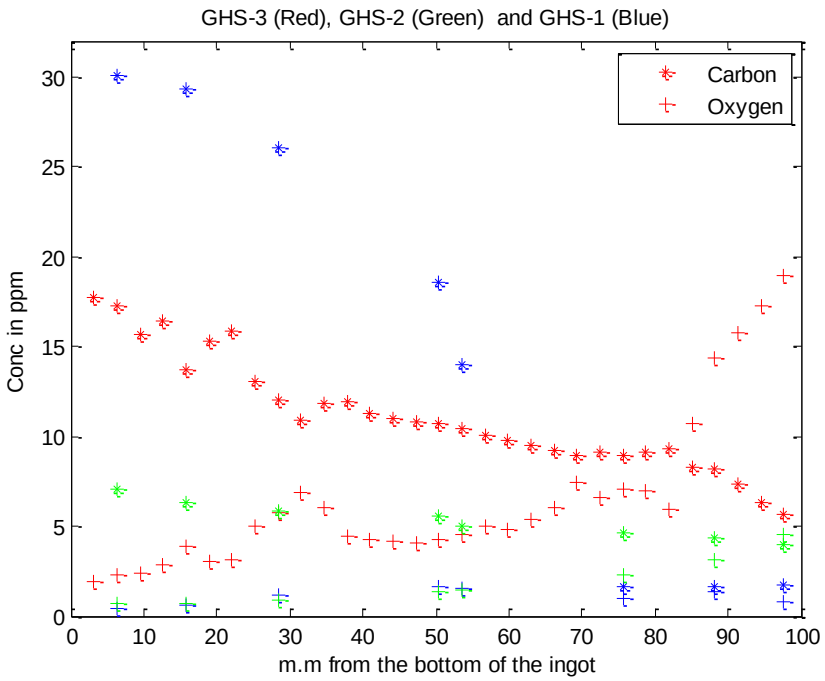

Fig 25

The diagram illustrates the combined concentrations of both oxygen and carbonic impurities of the three ingots. The ingots are distinguished with the same colors as the previous FTIR and PV scans curves. The combined concentrations of Oxygen and Carbon have their lowest values around 60-80 mm from the bottom in all the ingots.

The measured Oxygen and Carbon concentrations fit very well for the GHS3 and GHS2 ingots.

In the GHS1 measurements does the oxygen concentration decrease very abruptly around 40 to 50 mm and the carbon concentration is much lower than expected.

The reason for the deviations is due to problems with the Argon ventilation during the solidification process. It is suspected that the Argon ventilation has been out of order during the first 40-50 mm of the solidification process and then turned on again. This is probably also the reason why the carbon concentration decreases (instead of increasing) at the top of the GHS1 ingot.

The average Carbon and Oxygen concentrations would surely be much smaller in if there were no problems with the ventilation.

As remarked, it is very hard to determine the solubility limit of oxygen in silicon and many different values are found in literature. In the publication by M. Porrini et al, the amount of SiO_2 precipitates has been estimated as the difference in the oxygen concentration before and

after the wafers being annealed. Their results indicated that the density of bulk micro defects (BMD)/[cm^3] of SiO_2 precipitates increases logarithmically with the initial oxygen concentration and it is also very dependent on the thermal history of the ingot. This indicates that if there are oxygen precipitations in the ingots, the BMD density is probably much higher at the lowest 50 mm in the GHS2 ingot compared with the other ingot.

In further work it would be relevant to also perform FTIR measurements with other wavelengths of Carbon and Oxygen, for example SiO_2 precipitations which is detectable around 1220 cm^{-1} [51].

4.2 Germanium distribution

The initial concentration of germanium is 0,006% in the GHS3 ingot and 1% in the GHS1 ingot. The detection limit for germanium in silicon in the EPMA is 0,01% and the results are therefore uncertain for the GHS3 ingot.

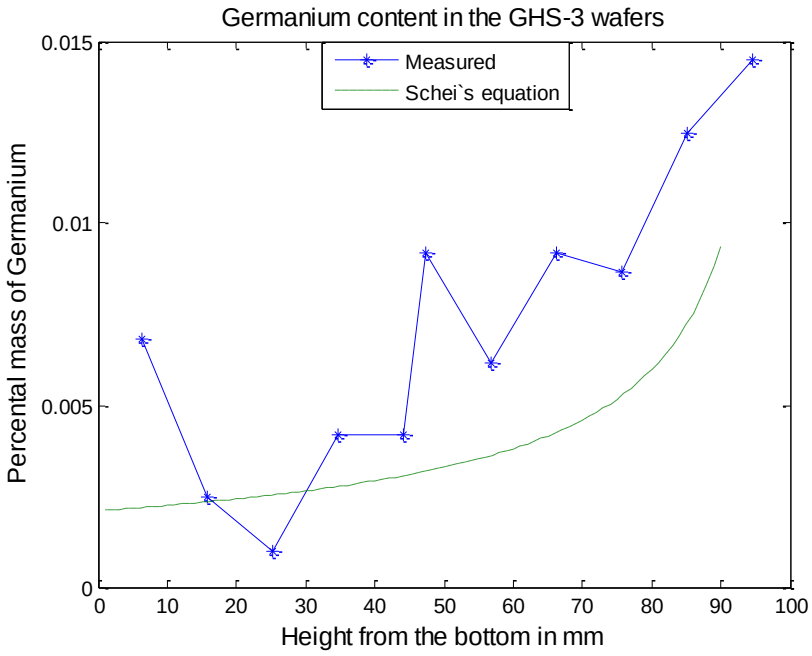

Figure 26

Almost all measured values of the Germanium concentration in the GHS3 ingot are below the expected values from the corresponding Scheil curve.

The values in figure 26 fit roughly with the corresponding Scheil curve. The reason why all detected values are a bit higher than expected is probably due to the low detection limit of the

EPMA. It is perhaps more true to consider the GHS3 ingot as a reference ingot than germanium doped due to the detection limit in the EPMA measurement.

The Germanium concentrations in the two measurements in the GHS1 ingot are pretty much in steady state up to 80 mm from the bottom. The outer measurement starts then to increase similar to the corresponding Scheil curve, disregard the abrupt oscillations at the top. The average Germanium concentration in the inner measurement (35 mm from center) is 0,83% and has an minimum and maximum value of 0,78 and 0.92% .

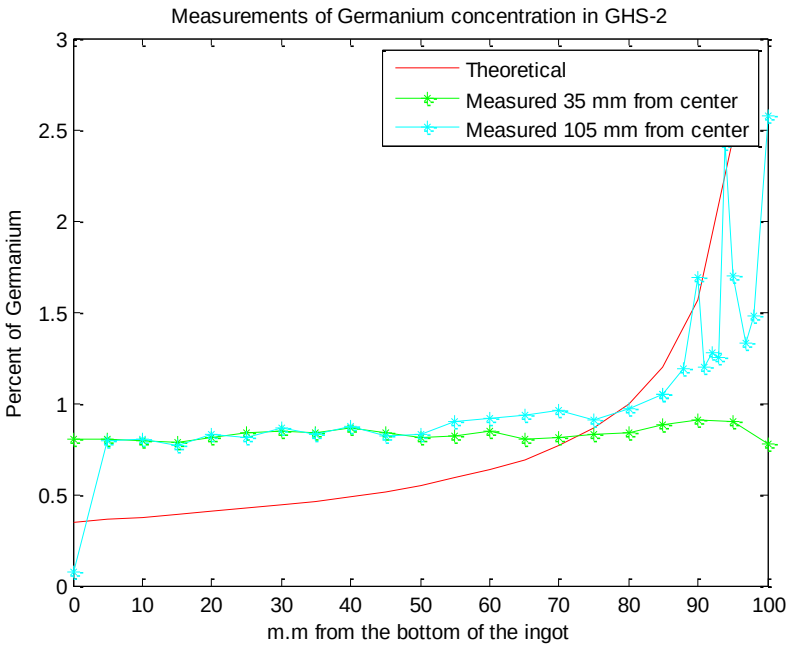

Figure 27

The germanium concentrations in the GH1 ingot

4.3 Dislocation density and distribution

Evaluation of PV-scan measurements is not always straightforward. What does the PV scan picture really illustrate? Normally it is useless to perform PV scan measurements on an un-etched wafer because the dislocations are too small to be detected. The chemical treatment in the etching process removes the weak bounded atoms around defects and exaggerates the size of them.

11 wafers from all the ingots were investigated with PV scan measurements and they are named due to their height from the bottom as illustrated in table 6:

Wafer number	Height from the bottom of the into [mm]
5	93.72
11	84.3
15	78.03
21	68.61
25	62.33
29	56.05
35	46.64
41	37.22
45	30.94
51	21.52
57	12.11

Table 6

Wafer 11 in the GHS3 ingot is replaced with wafer 13 which is located 25,54 mm from the bottom.

The total average amounts of dislocations from all the wafers in each ingot are summarized in table 7 below:

Ingot	Total amount of dislocations form all wafers	Average dislocation density per cm^2	Percental difference in dislocation density	Total amount of dislocations from all wafers after correction	Average dislocation density per cm^2 after correction	Percental difference in dislocation density after correction
GHS-1	$6,66 \cdot 10^7$	$3,78 \cdot 10^5$	Between GHS1 and GHS3: 45,41%	$6,33 \cdot 10^7$	$3,60 \cdot 10^5$	Between GHS1 and GHS3: 48,12%
GHS-2	$7,68 \cdot 10^7$	$4,36 \cdot 10^5$	Between GHS1 and GHS2: 13.21%	$7,81 \cdot 10^7$	$4,44 \cdot 10^5$	Between GHS1 and GHS2: 18.95% 1
GHS-3	$1,22 \cdot 10^8$	$6,93 \cdot 10^5$	Between GHS2 and GHS3: 37,05%	$1,22 \cdot 10^8$	$6,93 \cdot 10^5$	Between GHS2 and GHS3: 35,98%

Table7

Summation of all the dislocation from the PV scans measurements. Column 5 and 6 expresses the dislocation density PV scan pictures after adjustment as explained in Figure 28 below.

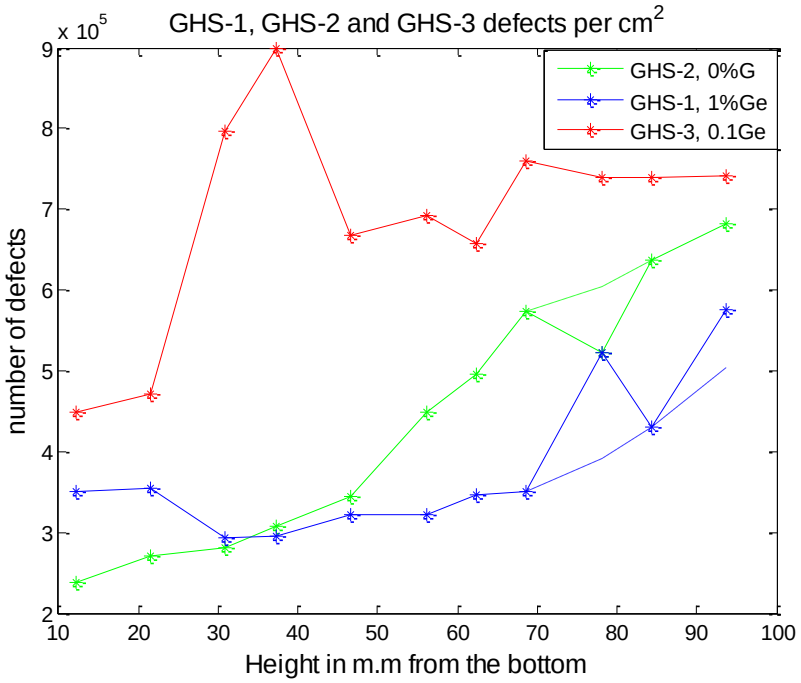

Figure 28

The dashed lines in the dislocation density curves are assumptions of the dislocation density according to probable sources of errors in the experiment.

In figure 28, two dashed lines are shown according to corrections in the PV scan images. The dislocation density of the third last measurement in the green curve, GHS2-15 decreases significant compared with its neighbor wafers. The GHS2-15 image indicates that the dislocation density should be much higher because the contours of the dislocations are very similar to its neighbor wafers, but lesser intense. The dislocations look a bit shaded and with weaker amplitude compared to GHS2-21 and GHS2-11. The dislocation densities in the GHS1-5 and GHS-15 images are overblown, because the grinding process has created scratches which are detected as dislocations.
In the GHS3 curve, the dislocation density rises very quickly in the GHS3-45 and GHS3-41 wafers. It is very hard due to the picture in attachment a) to determine if the rapid gradients depend on multiple twins or real dislocation in the GHS3 ingot.

The error analysis in figure 30 indicates that the areas with a higher dislocation density than 3.1×10^5 /cm^2 are reduced 10% to 50% in all three ingots.

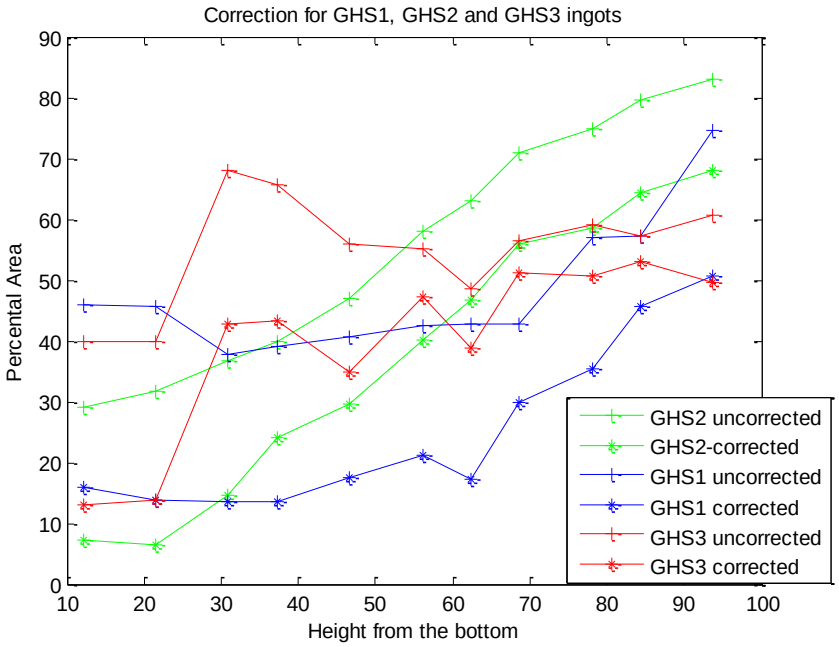

Figure 30

The error analysis of the PV scan image. The curves illustrates how many percent of the PV scanned area that contains a higher dislocation density than 3.1×10^5 /cm^2

The reductions of the dislocation areas are most important for wafers from the bottom of the ingots and become less remarkable at the top of the wafers. It is noteworthy that the reduction

of dislocations is more sufficient for the GHS1 ingot than the GHS2 ingot, especially at the lower parts of the ingots.

The GHS1 ingot has the lowest amount of dislocations and that must be a result of the germanium concentration. This difference in dislocation density is even more obvious with the error analysis in figure 30.
To evaluate the correspondence between the dislocation density and the Germanium content for the GHS3 ingot, we must keep in mind that the detection limit in the EPMA measurements is limited to 0,01%.
It is hard to observe any correspondence between Minozzi`s work, where 0.0155% of germanium was enough to reduce the dislocation density to maximum, with the results of the GHS3 ingot.
At the top of the GHS3 ingot, the germanium concentration reaches approximately the same optimum level as for Minozzia results and the dislocation density decreases slightly instead of increasing in figure 28. That could correspond with Minozzias work but the dislocation density goes up and down in several other intervals in the GHS3 curve.
The variable nature of the GHS3 dislocation curve in figure 28 shows that the dislocation density has probably been affected by perturbations in the solidification process and that the dislocation density does not always increases upwards in an ingot.
The weak intensity of the dislocation contours in the GHS2-15 wafer indicates the importance of the etching process in P.V scan measurements. Some thin wafers which were etched to be PV scanned for TEM preparation had the same problems with very low detection rate in the PV scan. This suggests that differences in the etching process might determine how the wafers are evaluated in the PV scan. Anyway, wafers from the GHS1 and GHS2 were etched in the same etching process and not be a major problem (opposite to the GHS3 ingot).
As described above, dislocations are generated from other dislocations through the so called Frank-Read source multiplication at the bottom of the ingot. The initial dislocation density is therefore very important for the total dislocation density and this must be taken into account while evaluating the dislocation density between all three ingots. The GHS1 ingot has 50%-100% higher (in regard to the error analysis) higher initial dislocation density compared to the GHS-2 ingot which probably depends due to variations in their thermal histories. It is then

likely that the difference of the total dislocation densities would be even more significant if the initial dislocation densities were more equal between the GHS1 and GHS2 ingots.
The dislocation density increases through the whole GHS2 ingot but decreases initially for the GHS1 ingot. This is likely to be explained, that the Germanium concentration prevented dislocations from further FRS-multiplications in the early part of the solidification but it cannot withstand the pressure higher up.
In further work, it would be desirable to study how the dislocation density is affected by changes in the etching process. Anyway, the author of this thesis has no experience of etching processes so proposal from more knowledgeable persons are of importance. No information about how the local shear moduli and local lattice parameter changes with germanium concentration in silicon has been found which would be good to know.
These investigations demands ultrapure Silicon because other impurities could affect the results.

4.4 Minority carrier lifetime measurements

The minority carrier lifetime results in table 8 and figure 31 illustrate large differences in the lifetimes between the GHS-1 and GHS-2 ingots and if the wafers are measured after being gettered or As cut. In general are the gettered lifetimes 50-90 μs for the GHS2 ingot and 5-25 μs for GHS1 ingot.

Wafer	As cut [μs]	Difference in lifetime compared with the previous value for the As cut values	Gettered [μs]	Difference in lifetime compared with the previous value for the Gettered cut values	Percental improvement in lifetime after being gettered. [%]	Height from bottom [mm]
GHS-1-12 (SiGe)	1.8	-	23.1	-	1183	81.62
GHS-2-12 (ref)	14.5	-	52.1	-	259	
GHS-1-26 (SiGe)	6.4	+4,6 μs	12.0	- 11,1μs	87,5	59.64
GHS-2-26 (ref)	12.0	-2,5 μs	75.3	+20,2 μs	527,5	
GHS-1-42 (SiGe)	4.7	-1,7μs against the GHS1-26 wafer. +2,9μs against the GHS1-12 wafer	5.3	-6,7μs against the GHS1-26 wafer. -17,8μs against the GHS1-12 wafer	12,76	34.53
GHS-2-42 (ref)	23.5	+9 μs against the GHS2-12 +11,5μs against the the GHS2-12 wafer	86.7	+11,4μs against the GHS1-26 wafer. +34,9μs against the GHS1-12 wafer	269	

Table 8: Average lifetime measured using MW-PCD. The pictures of the wafers after being investigated with the μw-PCD are illustrated in attachment c

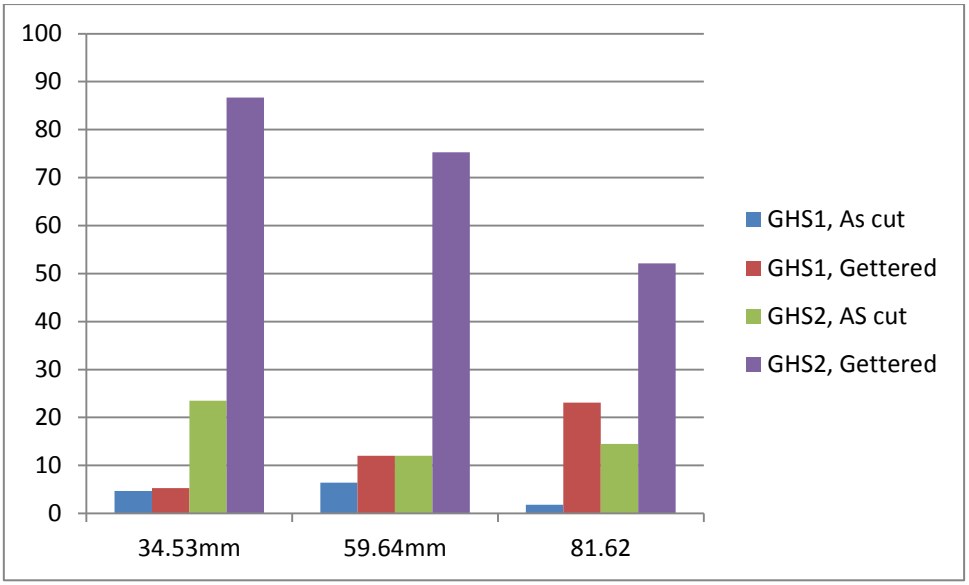

Figure 31

Graphical illustration of the data in table 8

Large areas of GHS-1-12 show lifetimes less than 1 µs in attachment c and significant improvement after the gettering process. Other wafers like GHS-1-26 and GHS-1-42 show less improvement. In general, the reference wafers respond better to the gettering process then the germanium doped ones, for example certain grains in GHS-2-42 lifetimes up to 200 µs.

The results of the lifetimes by A.G. Ulyashin et al in table 1 are much higher even at germanium concentrations up to 3-4% compared to the results for the GHS1 ingot.

An explanation could be that the higher amount of oxygen concentration in the lower part of the GHS1 ingot has influenced the lifetimes.

In the GHS1-42/26/12 are the oxygen concentrations around 30, 15 and 1,5 ppma and it is probably not a coincidence that the minority carrier increases with reducing oxygen concentration. In the gettering process, the minority carrier lifetimes increase very little for the GHS1-42-26 wafers but 4-5 times for the GHS2 ingot. The lower percentile enhancement for the GHS1 ingot might be explained that oxygen precipitates are unaffected by the gettering process. This is also in correspondence with the GHS1-12 wafer which shows extremely good improvement after the gettering process and has a very low oxygen concentration.

Previous work indicates that the minority carrier lifetime is very affected with the presence of oxygen precipitations.
If oxygen precipitates are present must the minority carrier lifetime in equation 8 be adjusted to:

Eq 12) $$\frac{1}{\tau_{eff}} = \frac{1}{\tau_b} + \frac{1}{\tau_{op}} + \frac{1}{\tau_s}$$

The lifetime of oxygen precipitate in equation 12 can be rewritten according to the radius as[52]:

Eq 13) $$\tau_{b_{op}} = \frac{1}{4\pi \cdot s_{eff} \cdot [BMD] \cdot \left(r_0^3 + 3Q_f \cdot r_0^2 / [B]\right)^{2/3}}$$

S_{eff} is the surface recombination velocity around the oxygen precipitation, BMD the Bulk Micro Defect density, r_o the radius of optical precipitations, Q_f (if the wafer is p-doped) is the positive charge density around oxygen precipitations and B is the dopant density.

According to M. Porrini et al, $\tau_{b_{op}}$ becomes very dominant at BMD around $10^{10}/cm^3$ which corresponded to an initial oxygen concentration 10 ppma (before the annealing processeses which supported the oxygen precipitations in their experiments)[53].
I had no opportunity to measure the SiO_2 concentration myself, but due to the fact, it is suspected that the oxygen precipitations are the major source for the reduction of the minority carrier lifetime in the GHS2 ingot.
Anyway, the improvements of the lifetimes in the gettered wafers indicates that both ingots contain none negligible amounts of impurities.

4.5 Internal quantum efficiency

Three wafers from the GHS1 and GHS2 ingots were performed with Light induced beam measurement, as illustrated in attachment d and presented in table in table 9 and figure 31.

Wafer	Average quantum efficiency[%]	Height from bottom [mm]
GHS-1-14 (SiGe)	90,46	78,48
GHS-2-16 (ref)	91,54	75,34
GHS-1-30 (SiGe)	82,69	53,36
GHS-2-30 (ref)	91,59	
GHS-1-52 (SiGe)	74	18,83
GHS-2-52 (ref)	92,39	

Table 9: The percentiles IQE`s are calculated from the raw data in attachment d. All none silicon parts in the attachment of the wafers are removed from the average values.

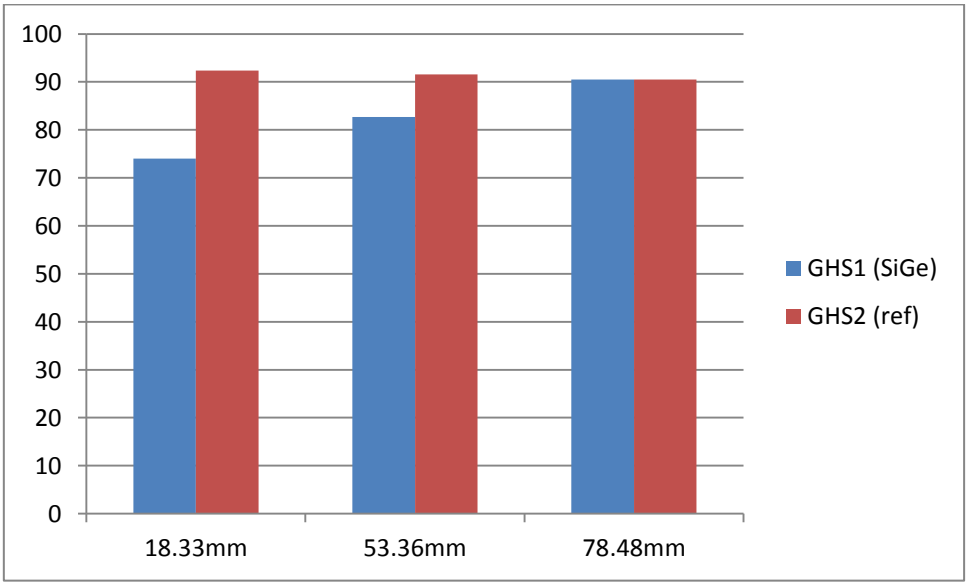

Figure 32

Graphical illustration of the data in table 9

The IQE features an almost steady state behaviour for the GHS2 ingot but increases with height for the GHS1 ingot. In attachment d, grain boundaries and dislocation clusters seem to be responsible for the major reduction of the IQE for the GHS1-14 and GHS2-16/30/52 wafers. In the GHS1-30/52 wafers, grain boundaries and dislocations are also present but the

major reduction looks to be more homogenously distributed all over the wafers, which indicates the presence of impurities and/or precipitations. The IQE in GHS1-14 (which has very low oxygen concentration compared to GHS1-30/52) is fully comparable with GHS2-16 and much better than the other wafers from the same ingot which indicates the importance of the higher oxygen concentration.
The lower minority carrier lifetimes in the GHS1-42/26 wafer and IQE in the GHS1-52/30 indicates a connection. The wafers are approximately from the same height in the GHS1 and reductions of the IQE and minority carrier seem to somewhat be proportional to the corresponding oxygen concentration in figure 23. GHS1-14 has also almost the same IQE as GHS2-16 which also support this idea.

4.6 Solar cell efficiency

The efficiencies, Open voltages V_{OC}, short circuit current J_{SC} and fill factor FF for the GHS1- and the GHS2-wafers are shown in Tables 10 and 11 and presented in figure 33 as well (only efficiency results are presented for the GHS3 wafers).
As explained many results, are not usable because of poor printing of the edges or short circuit.
The successful solar cells from the GHS2 ingot have in general efficiencies around 12% - 13% and the equivalent solar cells from the GHS1 ingot have efficiencies around 10% - 12%. Some solar cells at the top and the bottom of the ingots have very low efficiencies, around 1-2%. The efficiencies at the bottom of the GHS1 ingot are very low despite the good fill factors. The Solar cells from the GHS3 ingot exhibits very low values.

Height from the bottom	efficiency	Voc	Jsc	FF	Comment	GHS-3
97.31	8,991	0,5761	27,16	0,5746	poor printing	Efficiency
94.17	11,62	0,5899	27,58	0,7138		4,4
91.03	12,42	0,5918	28,22	0,744		
87.89	12,76	0,5958	28,82	0,7431		3,6
78.48	12,85	0,5951	29,2	0,7394		3,23
75.34	-	-	-	-	Broken	
65.92	7,245	0,5625	28,35	0,4543	edge isolation	4,79
62.78	12,27	0,5889	28,11	0,7416		
53.36	11,39	0,5771	26,84	0,7353		3,69
50.22	10,99	0,5712	25,74	0,7474		4,26
47.09	11,4	0,5763	26,47	0,7475		
43.95	10,6	0,5644	25,19	0,7459		
37.67	10,67	0,5679	25,38	0,7406		4,79
28.25	10,93	0,5688	25,68	0,7484		3,48
25.11	10,46	0,5671	25,5	0,7232		3,7
18.83	10,18	0,5594	25,02	0,7276		4,22
12.56	7,832	0,5305	20,22	0,7301	*	
9.42	5,731	0,4997	16,11	0,7119	*	2,69
6.28	4,694	0,4808	13,52	0,7224	*	
3.14	1,006	0,3046	13,12	0,2518	Shunted	

Table 10. Efficiency, Voc, Jsc and fill factor for GHS1 (GeSi samples). The GHS-3 solar cell efficiencies are presented in the last column. The blue tagging marks the wafers which are not affected by any faults from both the GHS2 and GHS1 ingots.

**** Low efficiency despite a FF of above 0.7.***

Height from the bottom	Efficiency	Voc	Jsc	FF	Comment	η =GHS2-GHS1
97.31					Broken	-6.5860
94.17	2,405	0,3234	28,66	0,2596	Shunted	-10.8308
91.03	0,7892	0,1244	25,84	0,2456	Shunted	-10.5540
87.89	1,866	0,2614	28,15	0,2536	Shunted	-6.3730
78.48	6,387	0,5345	29,11	0,4105	Shunted	-6.4630
75.34	3,025	0,4172	29	0,25	Shunted	--
65.92	13,12	0,5952	29,97	0,7357		5.8750
62.78	9,143	0,593	29,6	0,5209	poor edge isolation	-3.1270
53.36	12,48	0,55945	30,14	0,6967		1.0900
50.22	13,56	0,602	30,31	0,743		2.5700
47.09	13,57	0,6026	30,3	0,743		2.1700
43.95	13,43	0,6003	30,36	0,737		2.8300
37.67	13,75	0,6048	30,5	0,7455		3.0800
28.25	12,21	0,5872	30,08	0,6912		1.2800
25.11	13,54	0,6031	30,29	0,7413		3.0800
18.83	12,95	0,5899	30,24	0,7261		2.7700
12.56	13,35	0,6	30,1	0,7393		5.5180
9.42	13,04	0,5931	30,01	0,7324		7.3090
6.28	13,34	0,5973	30,05	0,743		8.6460
3.14	2,976	0,4085	28,46	0,256	Shunted	1.9700

Table 11. Efficiency, Voc, Jsc and fillfactor for GHS2 (Reference samples).

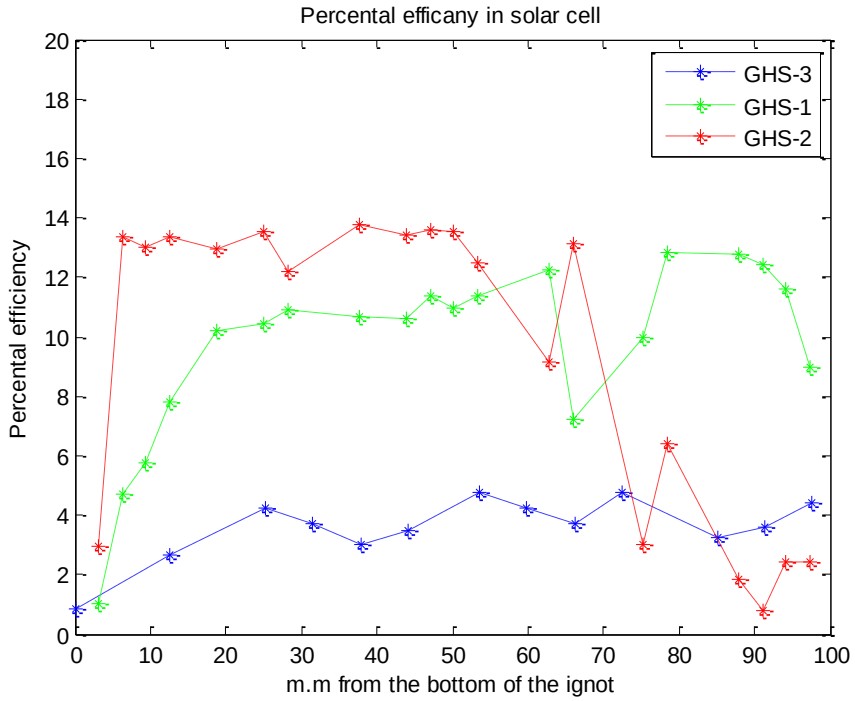

Figure 33

The efficiencies of the solar cells from the GHS1, GHS2 and GHS3ingots

The efficiencies are around 1-3% higher for solar cells from the GHS2 ingot compared to the GHS1 ingot. The minority carrier lifetime affects the solar cell efficiency as:[54]

Eq 14) $$\eta = \frac{V_{OC} I_{SC} FF}{P_{IN}} = \frac{\frac{nkT}{q} \ln\left(\frac{I_L}{I_0} + 1\right) \cdot q \cdot G\left(\sqrt{D_n \cdot \tau_n} + \sqrt{D_p \cdot \tau_p}\right) \cdot FF}{P_{IN}}$$

G is the generation rate

The differences in efficiencies between GHS1 and GHS2 differences are then not surprising due to the results of minority carrier lifetimes in table 8 and equation 14.

Due to the former discussions about the differences of minority carrier lifetimes and internal quantum efficiencies, the germanium concentration shall not be considered as the major source for the lower efficiencies in the GHS1 ingot compared to the reference ingot.
For example, the solar cell at 78,48 mm from the bottom in the GHS1 ingot has a very small oxygen concentration around 1,5 ppma and the efficiency of 12,85% which equal to most of the efficiencies in the GHS2 ingot. This again indicates that the efficiencies at the lower of the GHS1 ingot are reduced by oxygen precipitations.
Anyway we must remember that that the efficiencies are just measured from short flashes in the solar simulator and does not express how the light induced degradation affects the efficiencies. These experiments performed at IFE in Oslo but cancelled due to technical problems in the solar simulator.

The high fill factors in the three lowest solar cells in the GHS1 ingot indicate that these solar cells are not shunted and that the low efficiencies are caused by low J_{SC} and V_{OC}, which must be due to bulk recombination in the material itself. Former investigations by H.J Möller et al indicate that dislocations are often decorated by different oxygen precipitation. The combination of dislocations and oxygen precipitates reduces the minority carrier lifetime with the mechanism described in figure 16[55]. The three lowest solar cells in the GHS1 ingot are from the lowest 20 mm in the ingot. In the same region, the dislocation density is around 30% higher[‡] compared to the rest of the ingot where the oxygen concentration is still significant . The combination high of oxygen and dislocations concentrations could perhaps be the reason why the lower solar cells have remarkably lower efficiencies.

[‡] Remember that the dislocation density is measured from 12, 11 mm from the bottom of the ingot and the solar cell efficiencies 3.14 mm from the bottom. The real dislocation densities at the lowest solar cells are certainly higher than presented in figure 28.

In solar cells, the unwanted shunting effect occurs when a leakage current occurs between the P and N junctions. The leakage current is always more or less present in solar cells but heavily amplified by crystal defects or conducting impurities. It is not rare that the shunting effect occurs during the efficiency measurement in the solar simulator because the pressure by the metal (as seen in figure 20) makes the p and n layers into contact (it happened me several times at IFE). Dislocations can also be a source for increased leakage current.
Many more solar cells from the GHS2 ingot are subjected to short circuit than compared to the GHS1 ingot. It is hard to believe that the shunting effect is caused by precipitations because previous results indicates all kind of Oxygen and Carbon impurities are lowest at the upper part of the ingots.
The reason might be that the Germanium alloy has increased the yield strength and reduced the dislocation density of the GHS1 ingot enough to withstand the extra pressure better. This could imply that germanium doped solar cells have a much better quality and losses during the manufacture process than the reference cells

Germanium reminds pretty the same as silicon, both elements have 4 valence electrons, both are semiconductors and germanium can also work as a solar cell as well. Indeed germanium solar cells are used as an infrared tandem layer in multi-junction solar cells in space applications[56]. The theoretical efficiency limit or the *Schokley-Quisser limit*, with respect to the band gap in solar cells is expressed as:

Eq 15)
$$\eta = \frac{\int_{o}^{\lambda_G} \phi(\lambda)\frac{hc}{\lambda}d\lambda \cdot E_G \int_{0}^{\lambda_G} \phi(\lambda)d\lambda}{\int_{0}^{\infty} \phi(\lambda)\frac{hc}{\lambda}d\lambda \cdot \int_{o}^{\lambda_G} \phi(\lambda)\frac{hc}{\lambda}d\lambda}$$

Φ expresses the photon flux density, E_G is the band gap of the solar cell, λ_G is the excitation wavelength. By using data about the photon flux density it is possible to solve the equation numerically.

Germanium has a band gap of 0.67 eV[57] and the excitation wavelength of 1748 nm. With these constants, equation 15 indicates that the Schokley-Quisser limit for germanium solar

cells is around 20%[§] for an irradiance of 1000W/m^2. This efficiency is much lower than for silicon solar cells (33.7%). It is then likely that the band gap in a Si_{1-x}-Ge_x solar cell decreases with increasing germanium concentration which implies a lower theoretical efficiency for Ge-Si solar cells. In further work, investigations how the properties in Si_{1-x}-Ge_x solar cells are affected by different amounts of germanium are necessary. The author of this thesis could only find unreliable sources about that subject.

4.6 TEM examination

Due to limited time TEM analysis was limited but fortunately John Walmsley and I had time for one sample. The extensive preparation procedures for TEM were carried out for several samples but it was only possible to make a brief examination of a thin foil from sample GHS1-18, located 72.2 mm from the bottom of the ingot. The area which was prepared corresponds to the region in figure 22 where twinning was identified optically. The silicon sample is viewed down [110] so that a set of twin orientations are viewed edge-on. Two twin-related orientations are present in the field of view.

Figure 34

[§] The data about the photon flux was obtained by National Renewable laboratory at http://www.nrel.gov/solar_radiation/. The data is too extensive to attach.

This picture illustrates a part of a multiple twin with 3900 times magnification. The image in in the dark field mode and the twins are viewed as the dark and light fringes.

In figure 32, the diffraction image of the twins in figure 31 is shown. This shows clearly the superposition of the two twin related orientations of the [110] diffraction pattern.

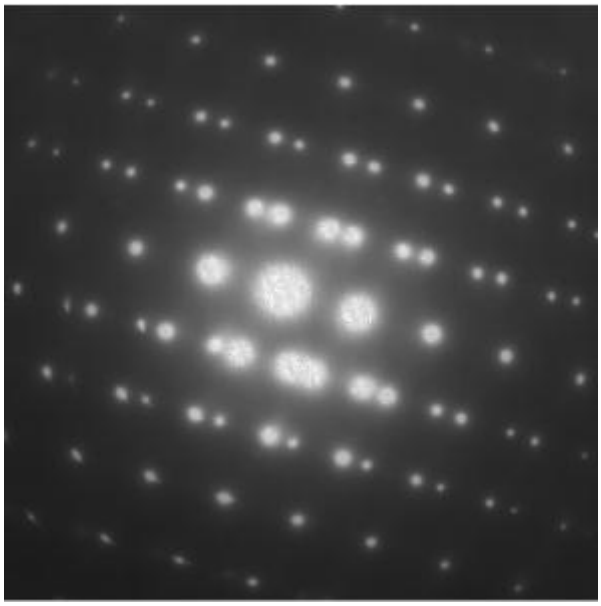

Figure 35

Figure 31 looks as a normal fcc diffraction pattern in the [110] disregard that most of the diffraction spots are divided into two adjacent spots[58].
The symmetry of the adjacent diffraction spots must be a connection between the crystal twins.

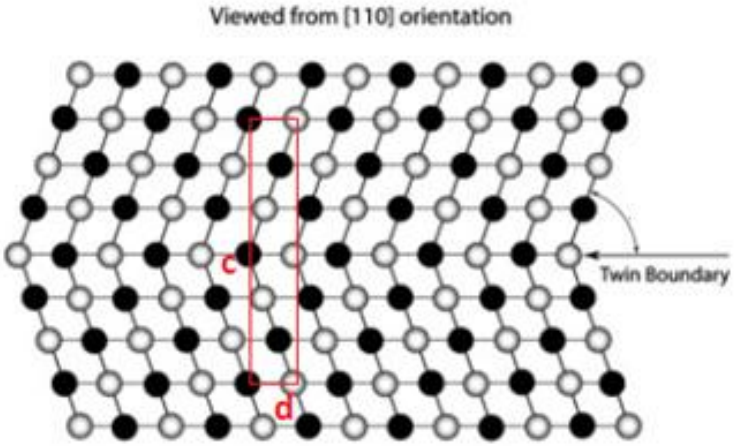

Figure 36

The figure illustrates the real space image of the (110) plane in the silicon FCC crystal structure. This image originates from the publication "Deformation twinning in nanocrystalline materials" Y.T. Zhu et al but has been modified with the red rectangle.

The line of single diffraction dots in the middle of figure 32 corresponds to the twin boundary as seen in figure 33.

The reciprocal distance between two adjacent diffraction spots is then in equal to a "*double Bragg diffraction*" between two symmetric atoms located on different sides of the twin boundary, indicated c in figure 33.

No kind of dislocations were observed in the sample that was examined. This was either not expected as the premier observation due to the lack of identify them optically.

5.1 Conclusions

The important conclusions in this thesis are resumed as:

1. 13-20% of the dislocation is at least reduced in silicon with germanium compared to reference ingot. The germanium concentration affects the minority carrier lifetime, IQE and solar cell efficiency only slightly.
2. The oxygen concentration has probably a huge effect on the minority carrier lifetime IQE and solar cell efficiency in the GHS1 ingot.
3. I think the most useful work which can be used by other in future is the error analysis for the dislocation density as presented in figure 19.

5.2 Summary and further work

The main goal with this thesis was to investigate if it is favourable or not to add germanium into silicon solar cell. It is impossible to answer that question with the short and insufficient data provided in this thesis. Almost all solar cells in the GHS1 ingot have lower efficiencies compared with the reference material but as described it is absolutely not evident it depend on the Germanium content. According to the results of Deren Yang et al it is already clear that a germanium concentration of 0.43% increases the efficiency with 0.5%, due to suppression light induced degradation.[59] But we must remember that this publication investigated czochralski silicon solar cells which are single crystalline and not multi crystalline as in this thesis

All publications I have read about Ge-Si are very independent and indicate different conclusions about the optimum germanium concentration to increase the solar cell efficiency. In further work I recommend to make a more structured and accurate investigation where oxygen and carbons and other defects are avoid as much as possible. In this thesis I had only access to two different concentrations and many more investigation (including light induced

degradation investigations) in the interval between 0.01%-2% should be done to survey the optimum germanium concentration to increase the solar cell efficiency.

Attachment a) P.V scan image

GHS3-5 (93.72mm from bottom)

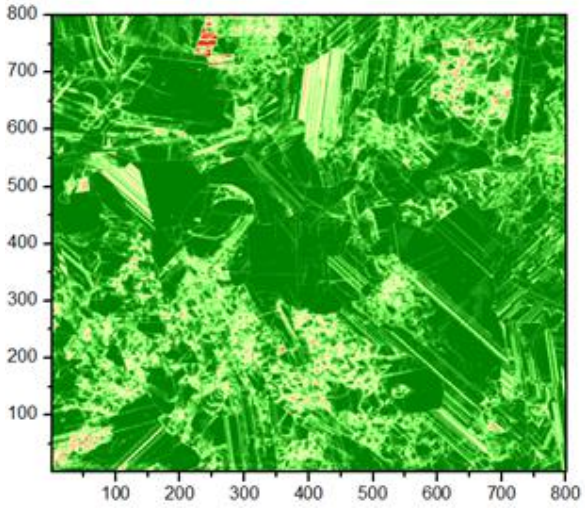

GHS2-5

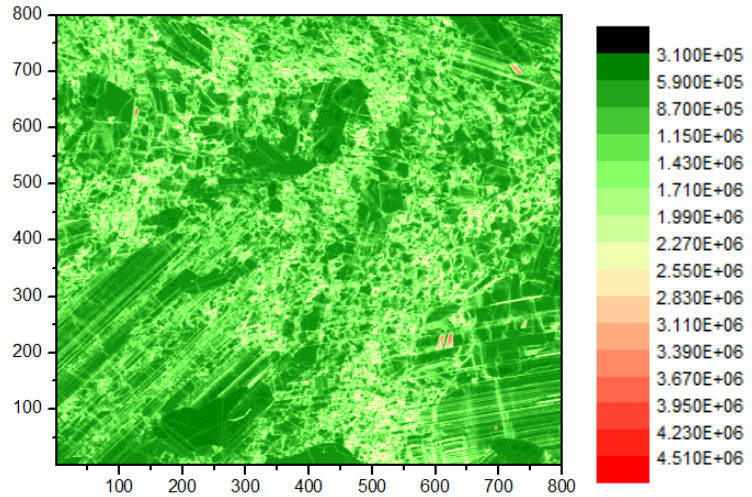

GHS1-5

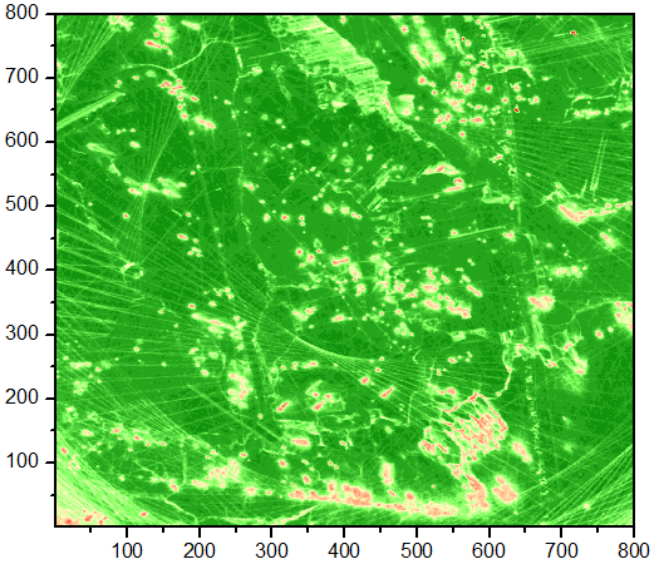

GHS3-11 (84.30 mm from the bottom)

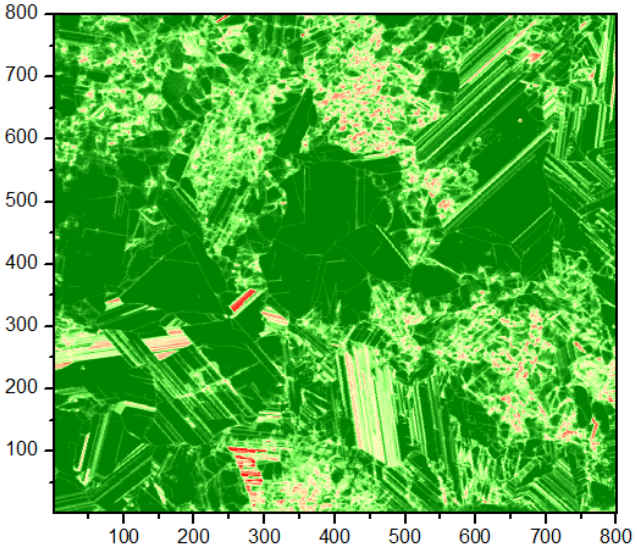

GHS2-11

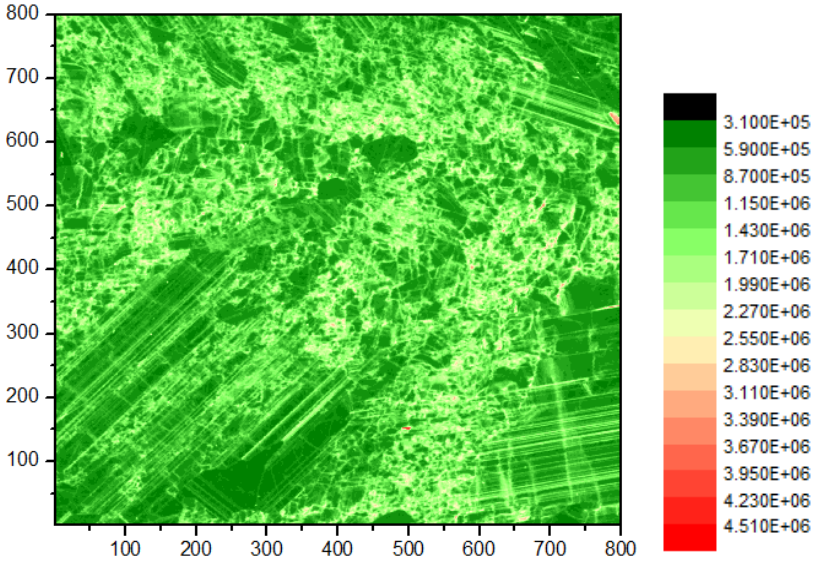

GHS1-11

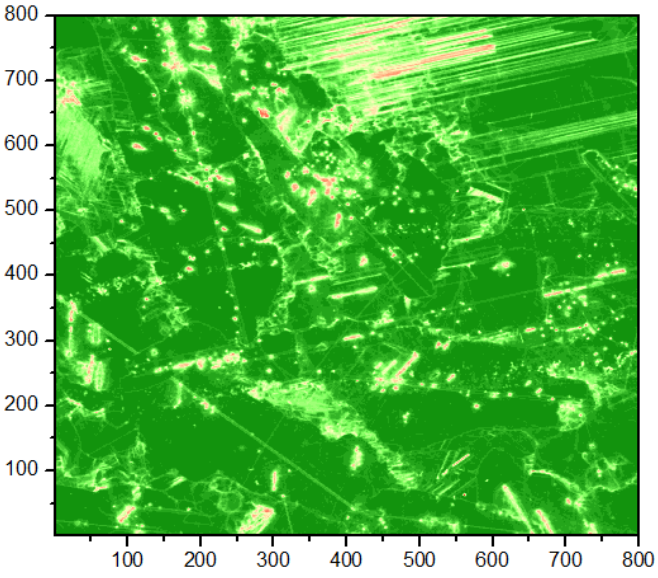

GHS3-15 (78.03 mm from the bottom)

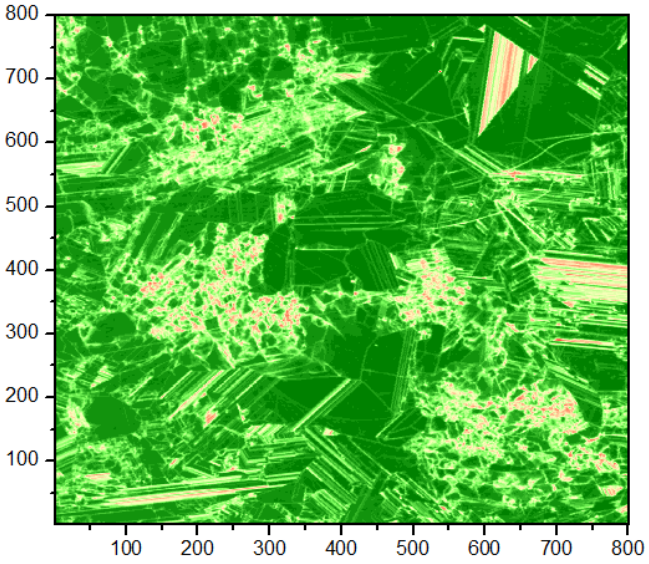

GHS2-15

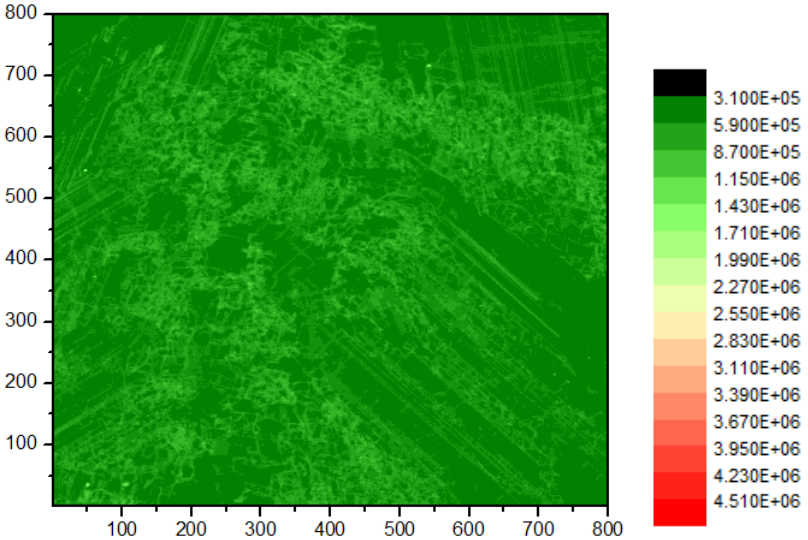

GHS1-15

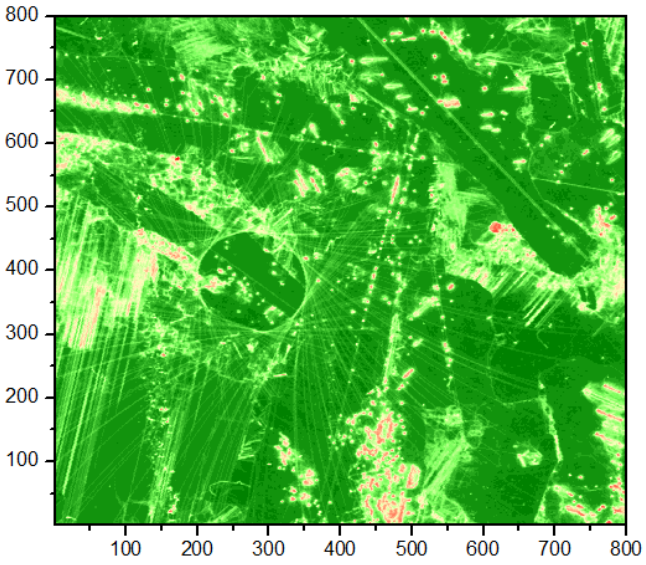

GHS3-21 (68.61 mm from the bottom)

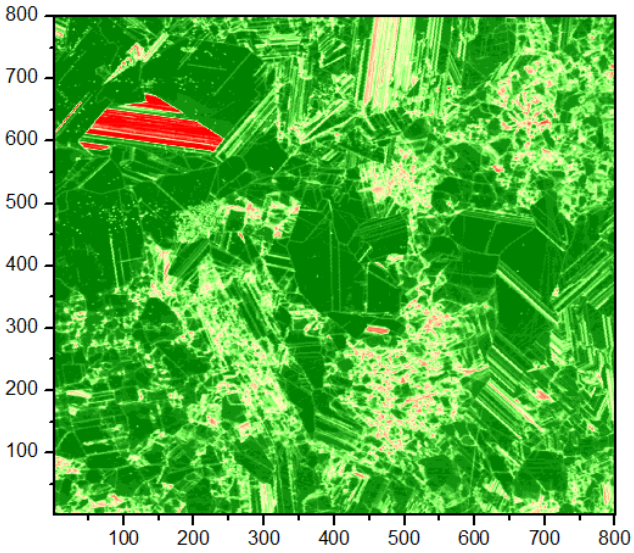

GHS2-21

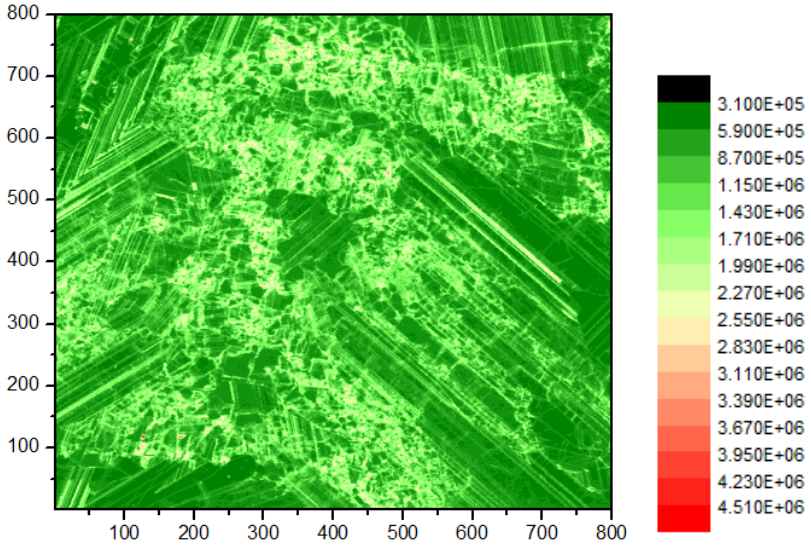

GHS1-21

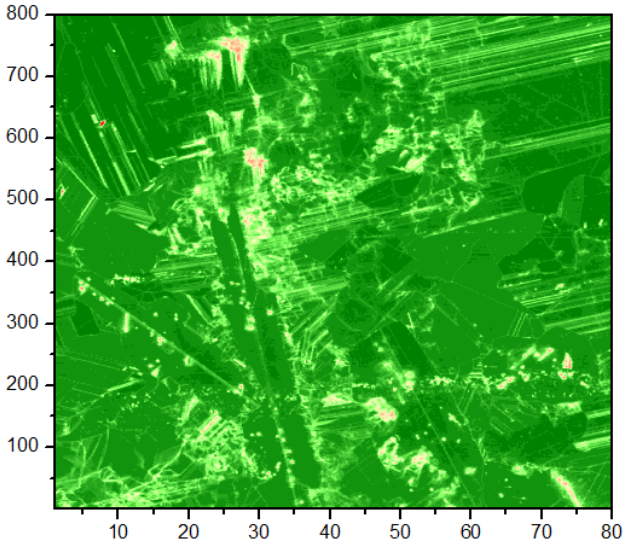

GHS3-25 (62.33 mm from the bottom)

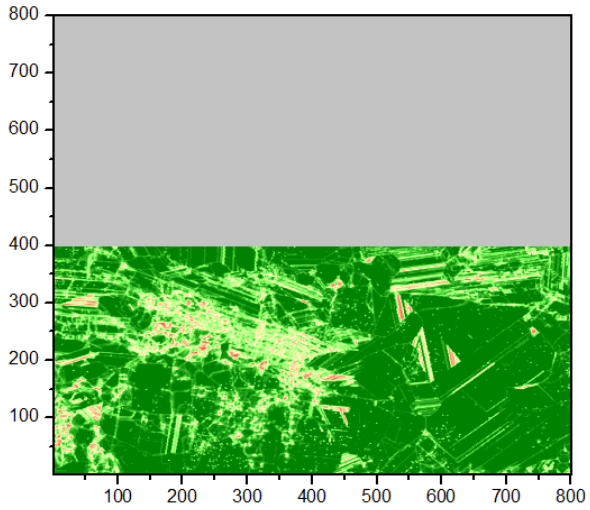

GHS2-25

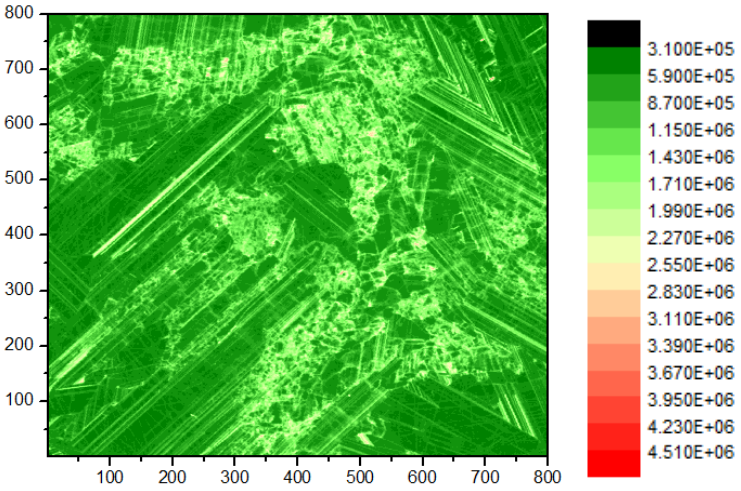

GHS1-25

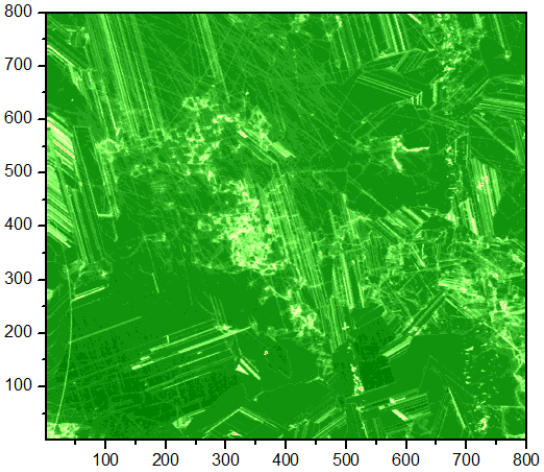

GHS3-29 (56.05 mm from the bottom)

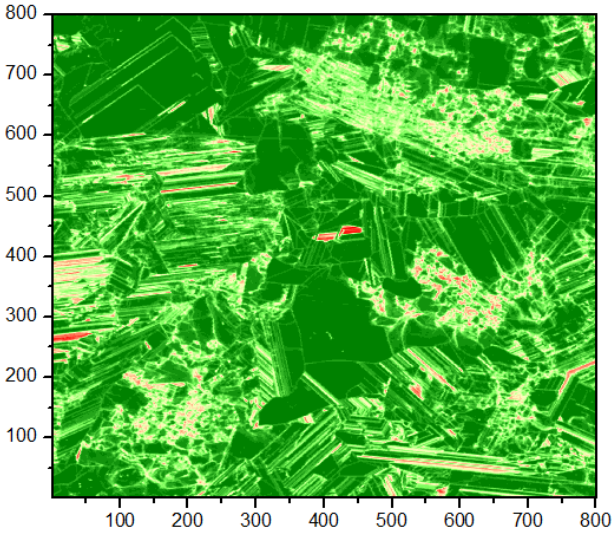

GHS2-29

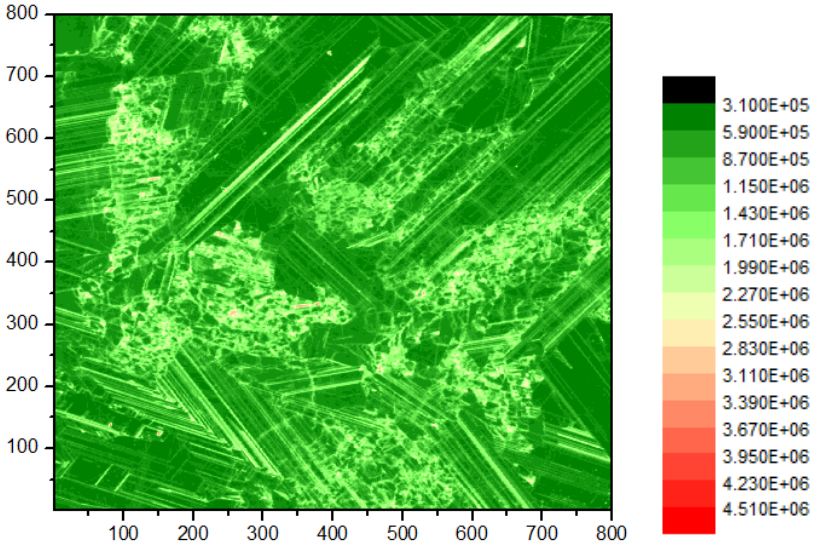

GHS1-29

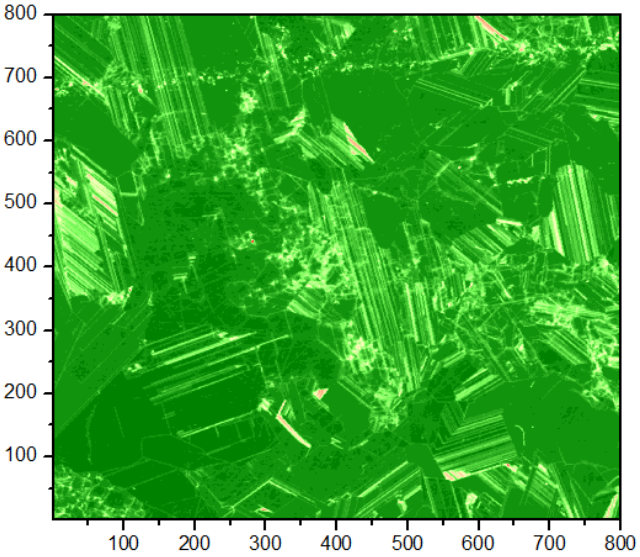

GHS3-35 (46.64 mm from the bottom)

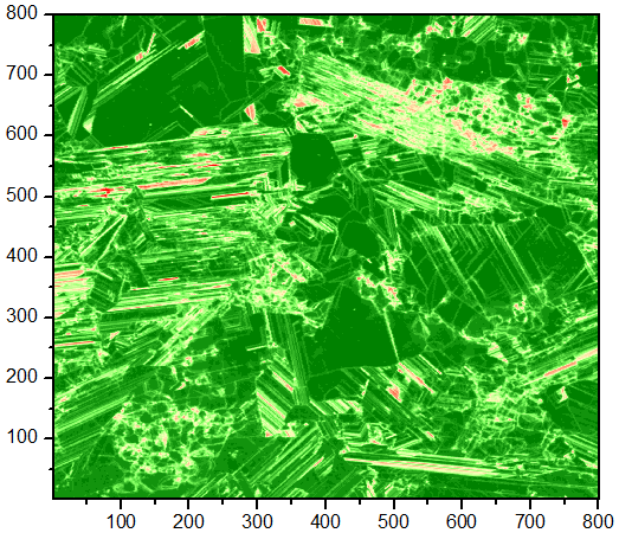

GHS2-35

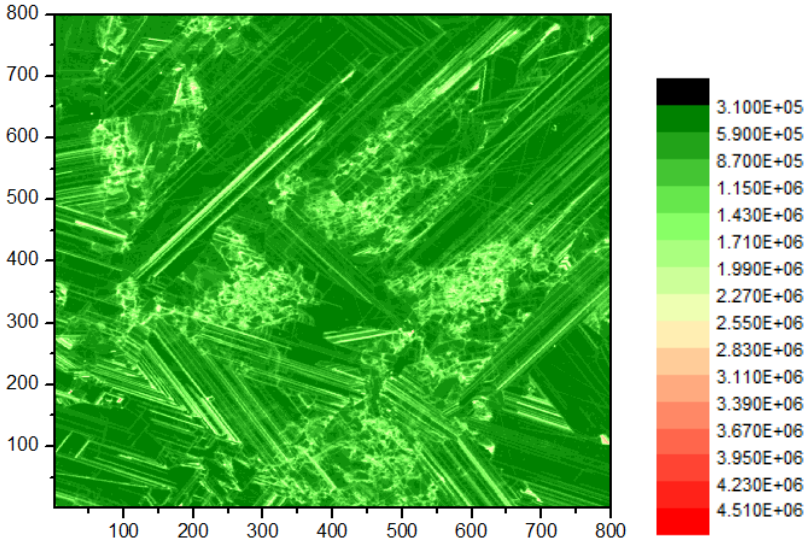

GHS1-35

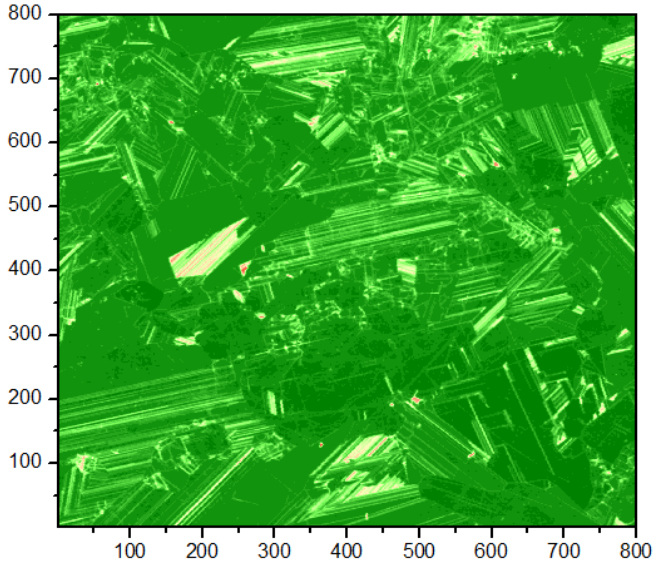

GHS3-41 (37.22 mm from the bottom)

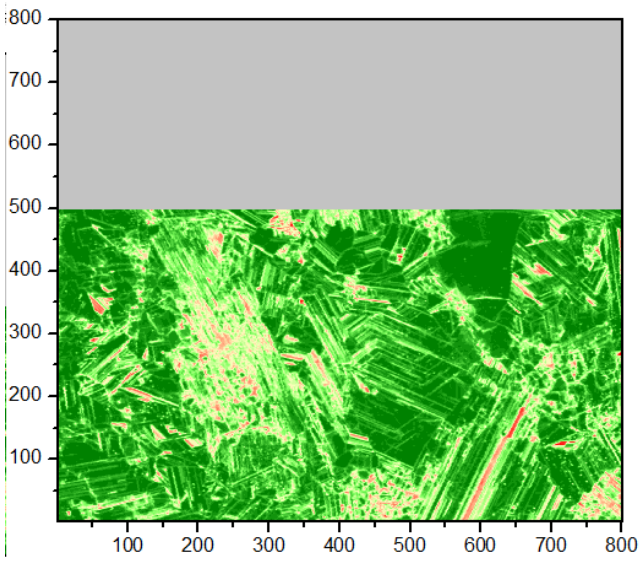

GHS2-41

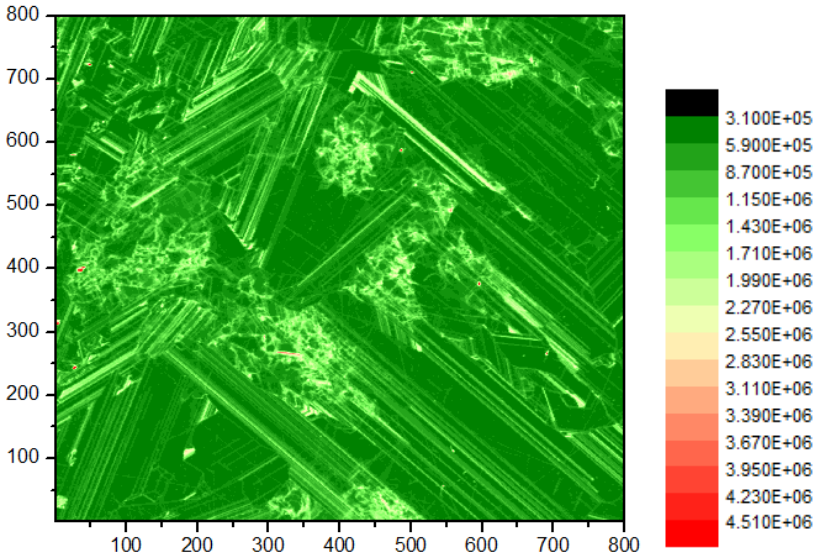

GHS1-41

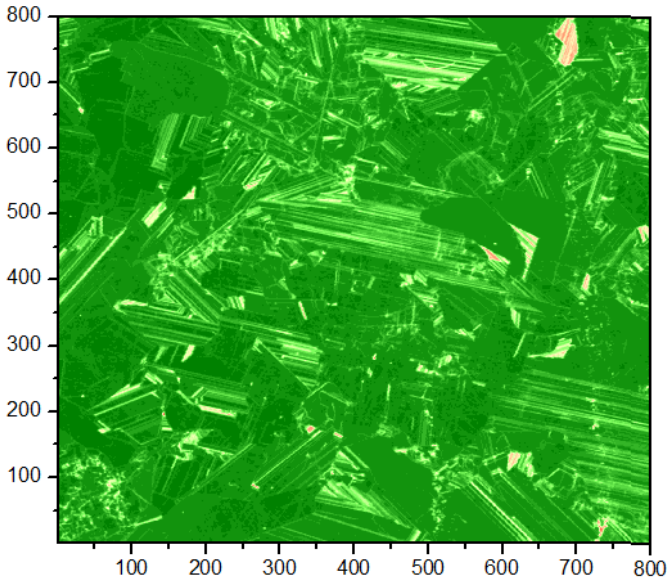

GHS3-45 (30.94 mm from the bottom)

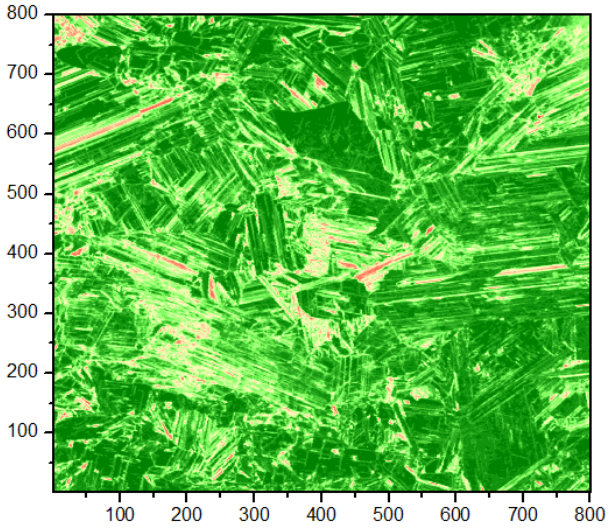

GHS2-45

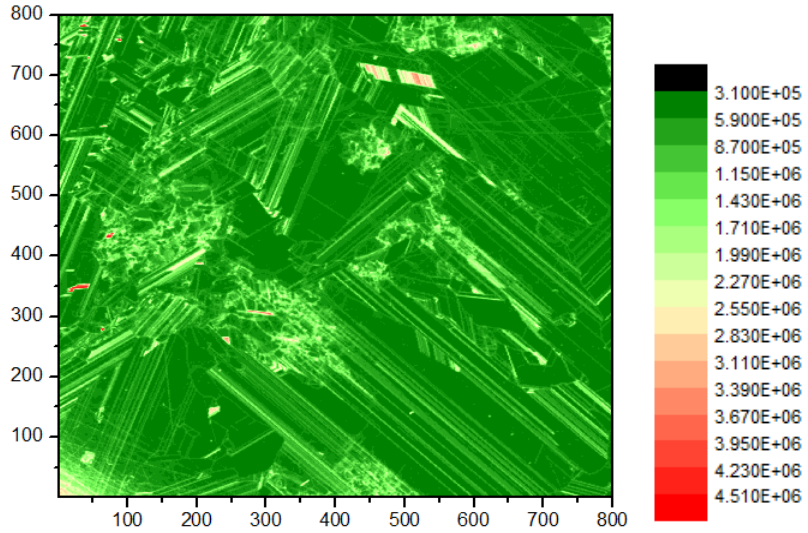

GHS1-45

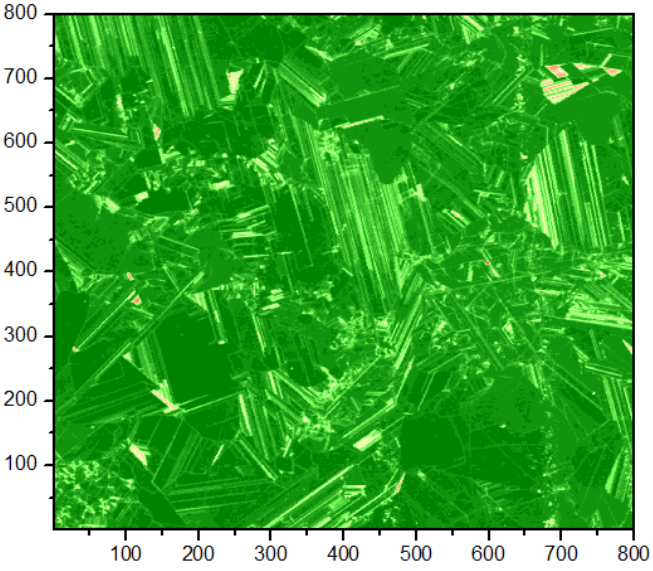

GHS3-51 (21.52 mm from the bottom)

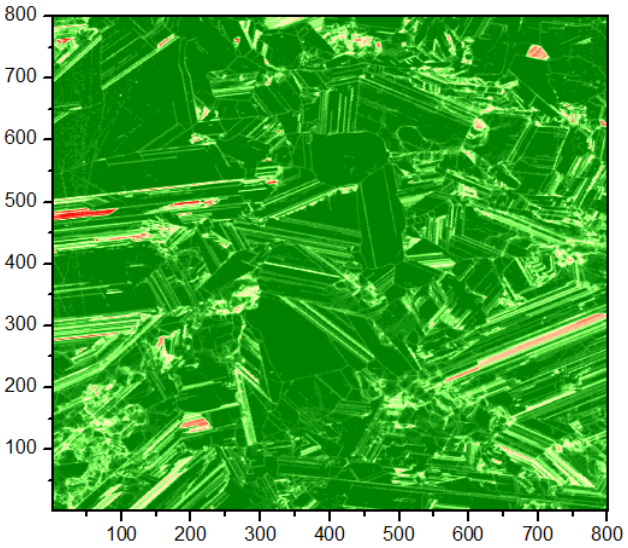

GHS2-51

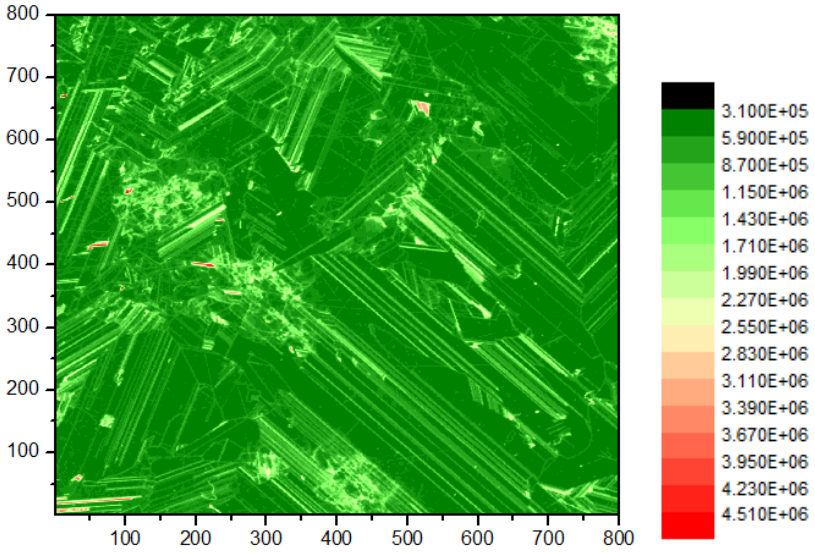

GHS1-51

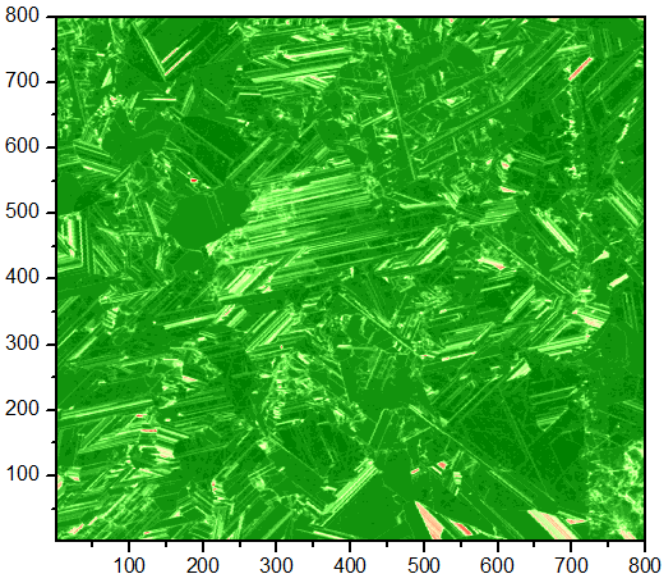

GHS3-57 (12.11 mm from the bottom)

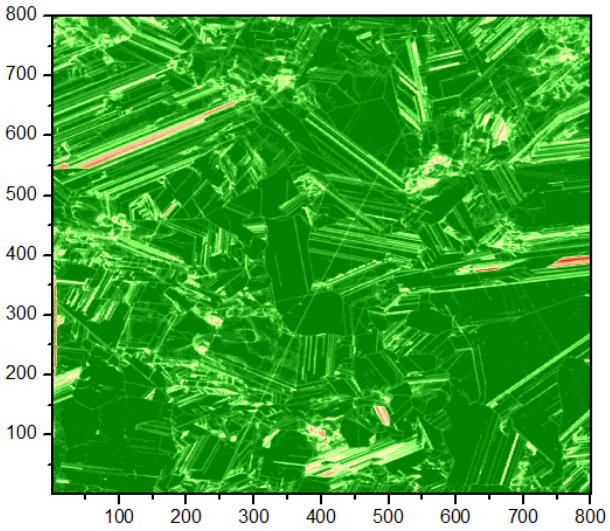

GHS2-57

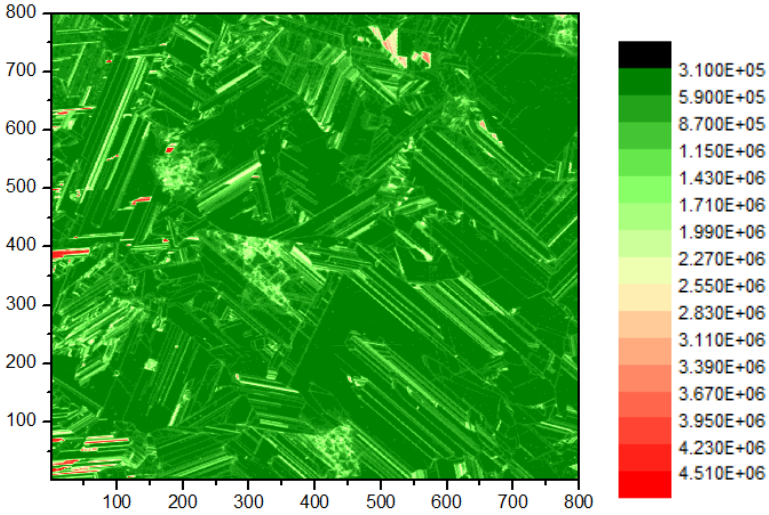

GHS1-57

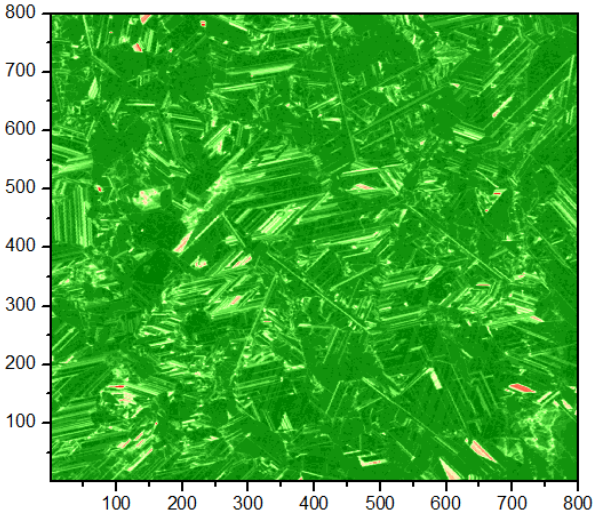

Attachment b) Height of all the wafers

TOP	bis Höhe [mm]	as-cut	SiGe	Referenz
1	100.00	Scheibe	GHS-1-1	GHS-2-1
2	97.31	Wafer	GHS-1-2	GHS-2-2
3	96.86	Scheibe	GHS-1-3	GHS-2-3
4	94.17	Wafer	GHS-1-4	GHS-2-4
5	93.72	Scheibe	GHS-1-5	GHS-2-5
6	91.03	Wafer	GHS-1-6	GHS-2-6
7	90.58	Scheibe	GHS-1-7	GHS-2-7
8	87.89	Wafer	GHS-1-8	GHS-2-8
9	87.44	Scheibe	GHS-1-9	GHS-2-9
10	84.75	Wafer	GHS-1-10	GHS-2-10
11	84.30	Scheibe	GHS-1-11	GHS-2-11
12	81.62	Wafer	GHS-1-12	GHS-2-12
13	81.17	Scheibe	GHS-1-13	GHS-2-13
14	78.48	Wafer	GHS-1-14	GHS-2-14
15	78.03	Scheibe	GHS-1-15	GHS-2-15
16	75.34	Wafer	GHS-1-16	GHS-2-16
17	74.89	Scheibe	GHS-1-17	GHS-2-17
18	72.20	Wafer	GHS-1-18	GHS-2-18
19	71.75	Scheibe	GHS-1-19	GHS-2-19
20	69.06	Wafer	GHS-1-20	GHS-2-20
21	68.61	Scheibe	GHS-1-21	GHS-2-21
22	65.92	Wafer	GHS-1-22	GHS-2-22
23	65.47	Scheibe	GHS-1-23	GHS-2-23
24	62.78	Wafer	GHS-1-24	GHS-2-24
25	62.33	Scheibe	GHS-1-25	GHS-2-25
26	59.64	Wafer	GHS-1-26	GHS-2-26
27	59.19	Scheibe	GHS-1-27	GHS-2-27
28	56.50	Wafer	GHS-1-28	GHS-2-28
29	56.05	Scheibe	GHS-1-29	GHS-2-29
30	53.36	Wafer	GHS-1-30	GHS-2-30
31	52.91	Scheibe	GHS-1-31	GHS-2-31
32	50.22	Wafer	GHS-1-32	GHS-2-32
33	49.78	Scheibe	GHS-1-33	GHS-2-33
34	47.09	Wafer	GHS-1-34	GHS-2-34
35	46.64	Scheibe	GHS-1-35	GHS-2-35
36	43.95	Wafer	GHS-1-36	GHS-2-36
37	43.50	Scheibe	GHS-1-37	GHS-2-37
38	40.81	Wafer	GHS-1-38	GHS-2-38
39	40.36	Scheibe	GHS-1-39	GHS-2-39
40	37.67	Wafer	GHS-1-40	GHS-2-40
41	37.22	Scheibe	GHS-1-41	GHS-2-41
42	34.53	Wafer	GHS-1-42	GHS-2-42
43	34.08	Scheibe	GHS-1-43	GHS-2-43
44	31.39	Wafer	GHS-1-44	GHS-2-44
45	30.94	Scheibe	GHS-1-45	GHS-2-45
46	28.25	Wafer	GHS-1-46	GHS-2-46
47	27.80	Scheibe	GHS-1-47	GHS-2-47
48	25.11	Wafer	GHS-1-48	GHS-2-48
49	24.66	Scheibe	GHS-1-49	GHS-2-49
50	21.97	Wafer	GHS-1-50	GHS-2-50
51	21.52	Scheibe	GHS-1-51	GHS-2-51
52	18.83	Wafer	GHS-1-52	GHS-2-52
53	18.38	Scheibe	GHS-1-53	GHS-2-53
54	15.70	Wafer	GHS-1-54	GHS-2-54
55	15.25	Scheibe	GHS-1-55	GHS-2-55
56	12.56	Wafer	GHS-1-56	GHS-2-56
57	12.11	Scheibe	GHS-1-57	GHS-2-57
58	9.42	Wafer	GHS-1-58	GHS-2-58
59	8.97	Scheibe	GHS-1-59	GHS-2-59
60	6.28	Wafer	GHS-1-60	GHS-2-60
61	5.83	Scheibe	GHS-1-61	GHS-2-61
62	3.14	Wafer	GHS-1-62	GHS-2-62
63	2.69	Scheibe	GHS-1-63	GHS-2-63

Attachment c) minority carrier lifetime experiments

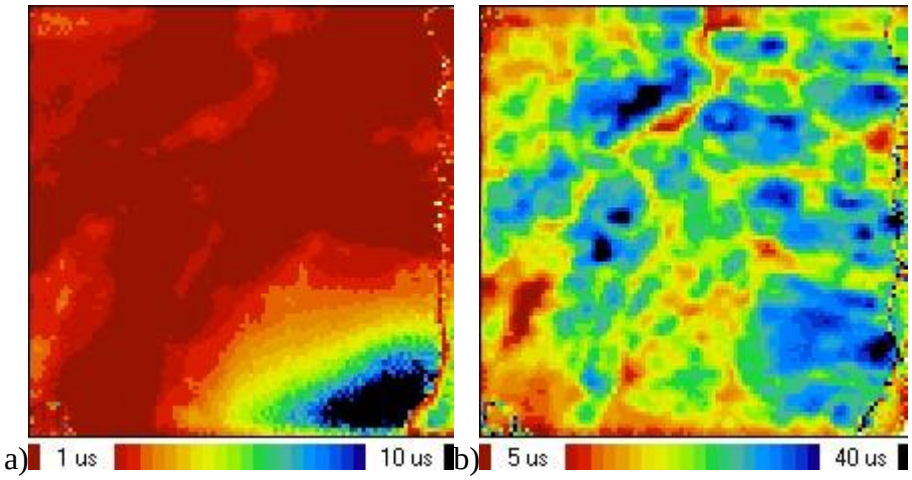

Figure 1. Lifetimes measured using MW-PCD for a) as cut and b) gettered wafer GHS-1-12.

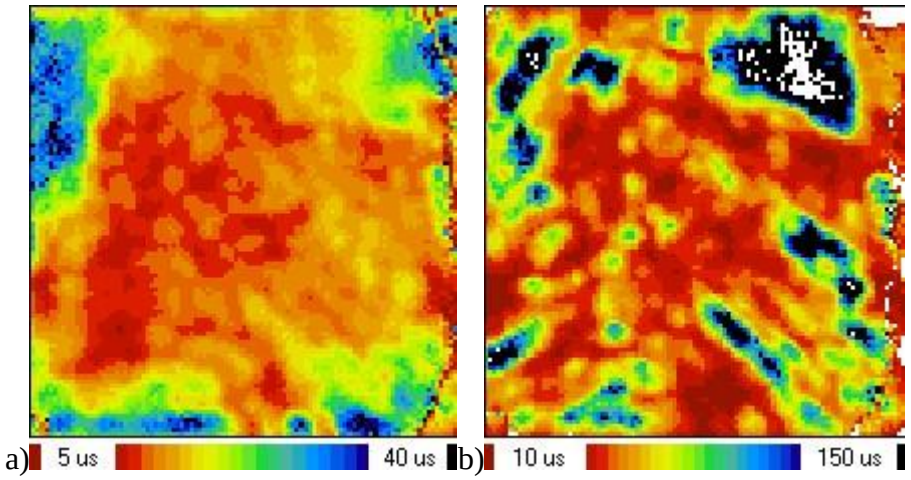

Figure 2. Lifetimes measured using MW-PCD for a) as cut and b) gettered wafer GHS-2-12.

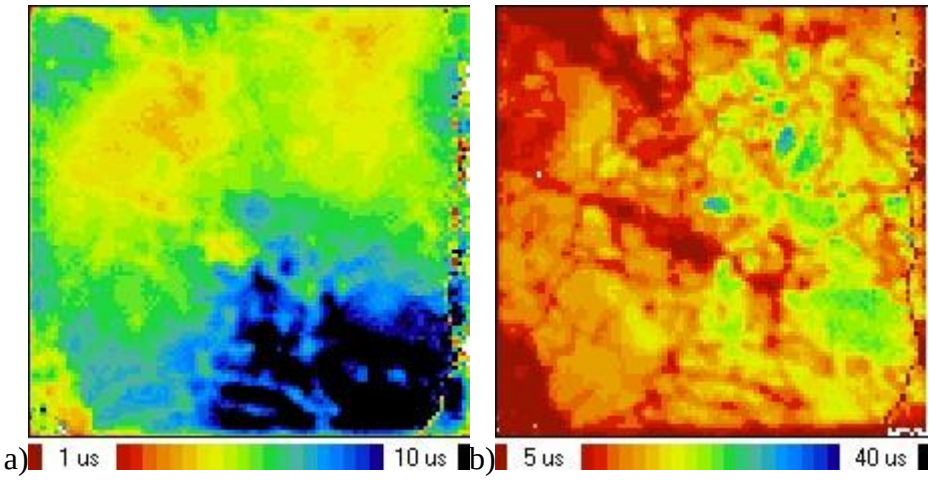

Figure 3. Lifetimes measured using MW-PCD for a) as cut and b) gettered wafer GHS-1-26.

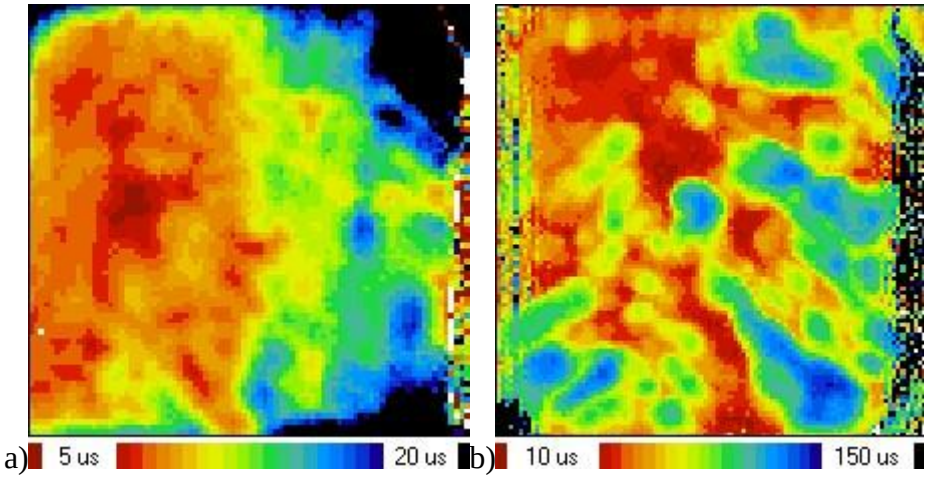

Figure 4 Lifetimes measured using MW-PCD for a) as cut and b) gettered wafer GHS-2-26.

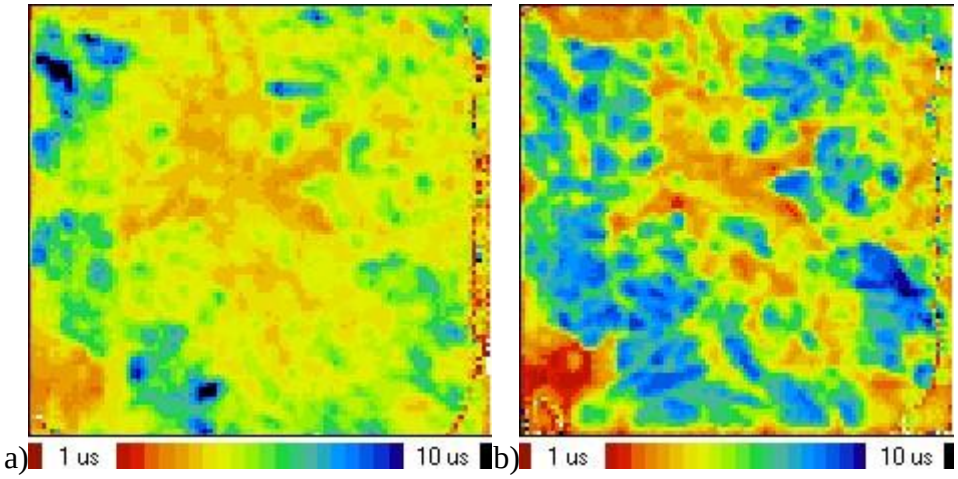

Figure 5. Lifetimes measured using MW-PCD for a) as cut and b) gettered wafer GHS-1-42.

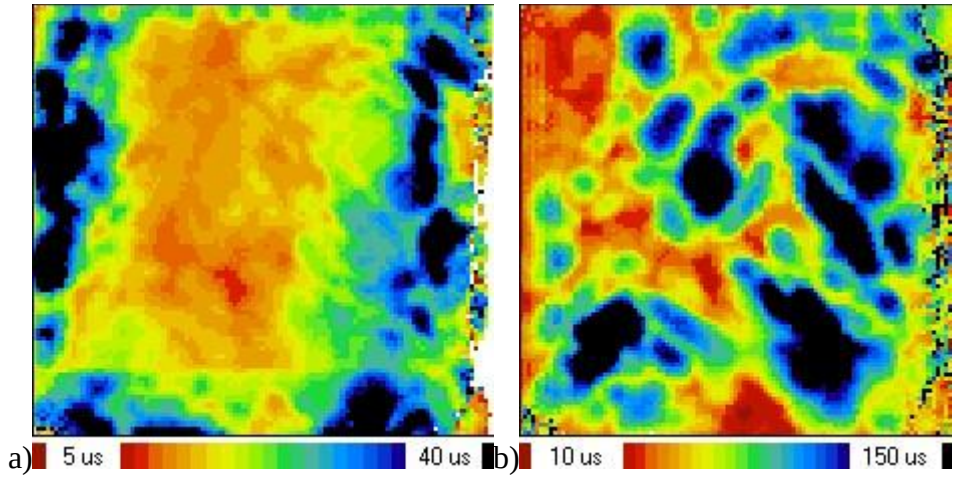

Figure 6. Lifetimes measured using MW-PCD for a) as cut and b) gettered wafer GHS-2-42.

Attachment d) Internal quantum efficiency

GHS1-14 (78,48 mm from the bottom)

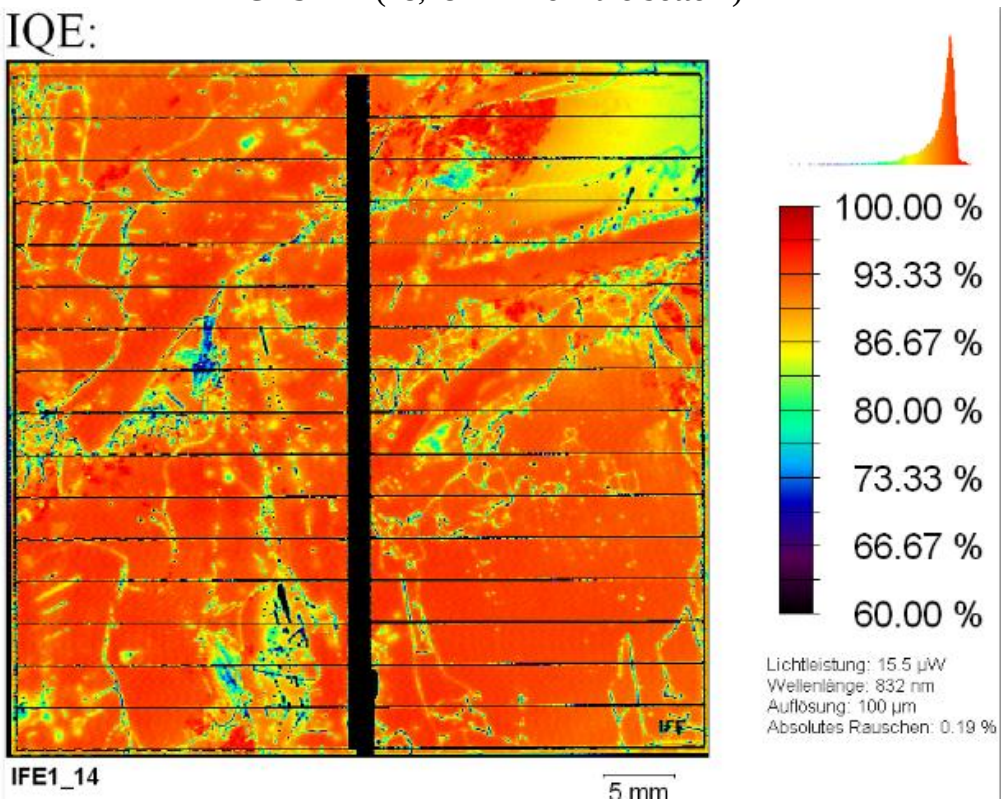

GHS2-16 (75.34 mm from the bottom)

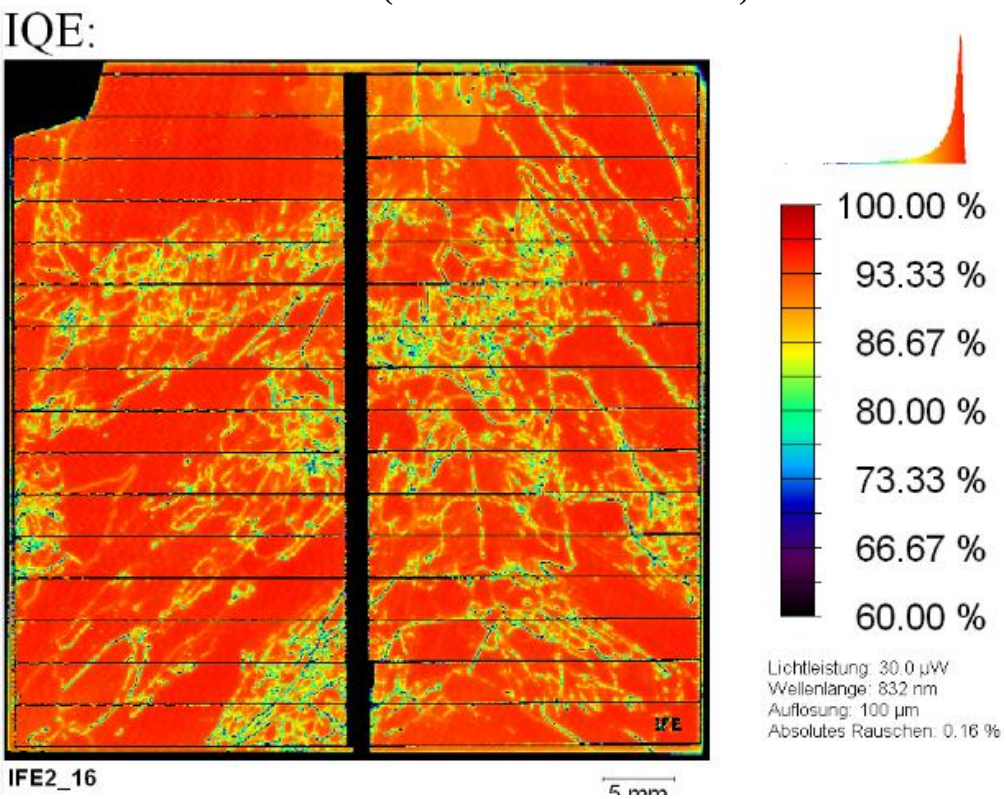

GHS1-30 (53,36 mm from the bottom)

IQE:

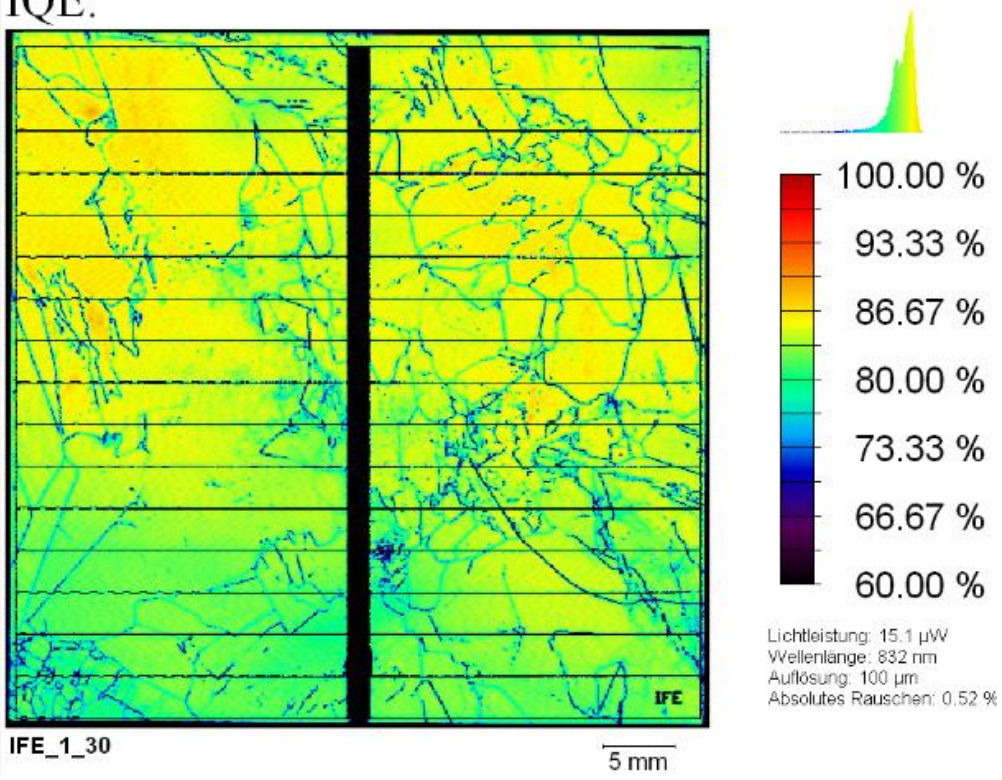

GHS2-30 mm from the bottom

IQE:

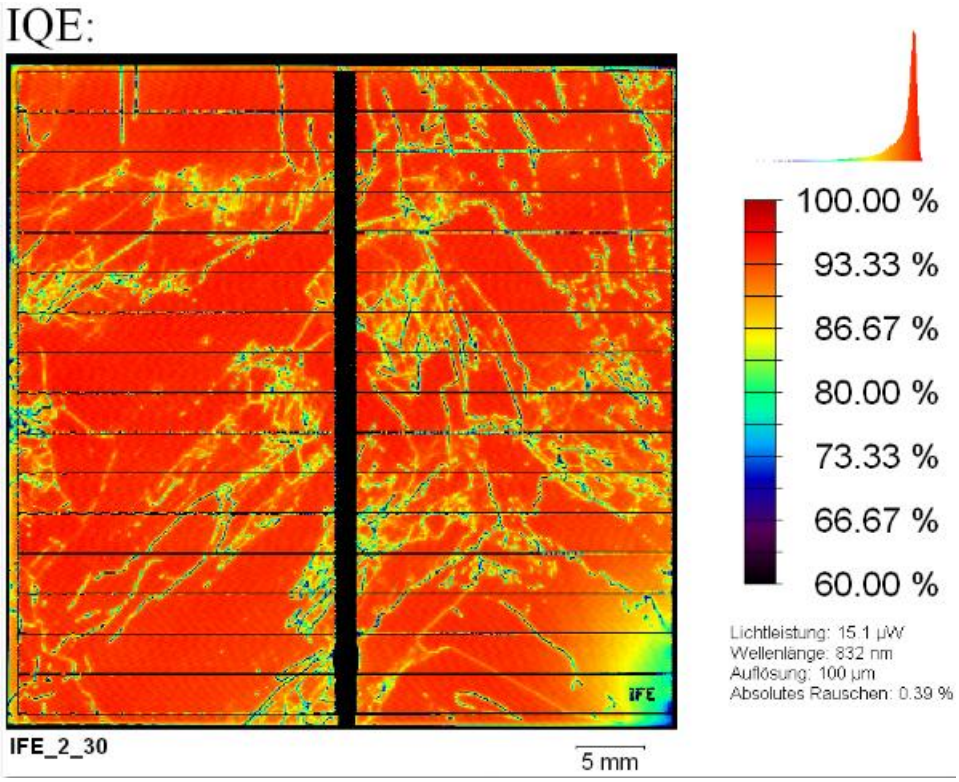

GHS1-52 (18.83 mm from the bottom)

IQE:

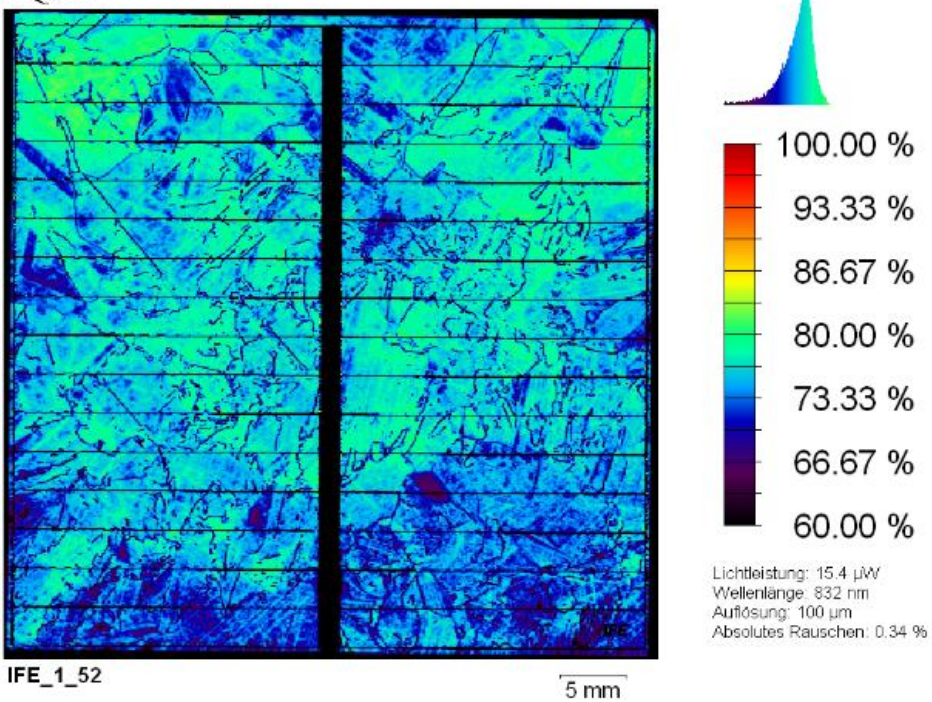

GHS2-52

IQE:

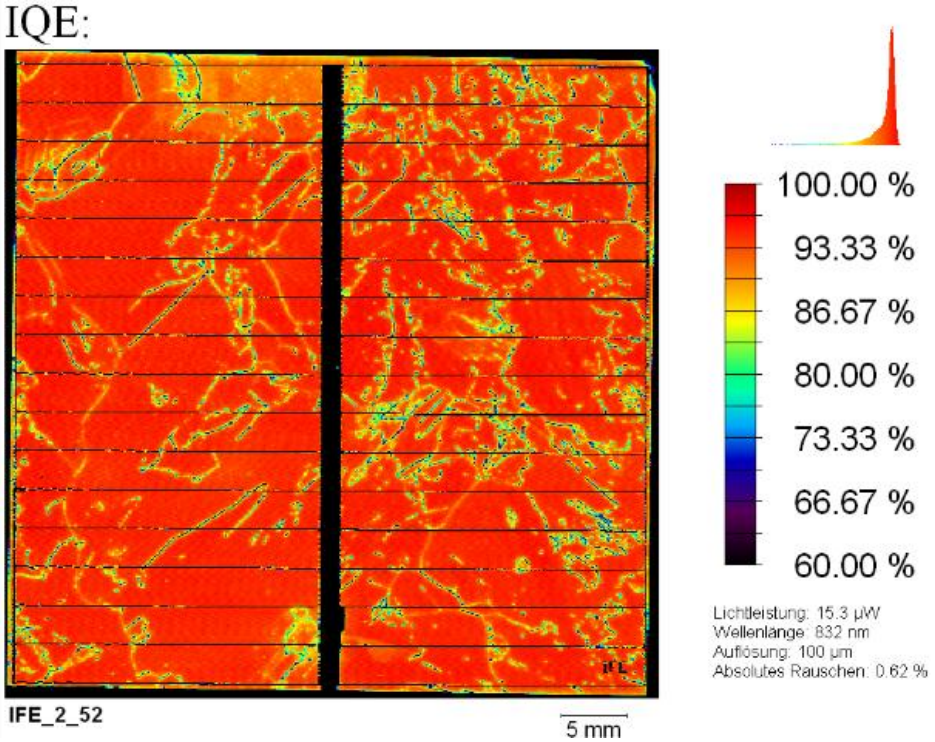

6 References

6.1 Figures

Figure 1: Made by Martin Bellman Ph.D. researcher at Sintef, Trondheim
Figure 2: http://biointerface.org/nano/templates/silicon/
Figure 3: http://www.tf.uni-kiel.de/matwis/amat/semitech_en/index.html
Figure 4: http://www.ndted.org/EducationResources/CommunityCollege/Materials/Structure/point_defects.htm
Figure 5: http://www.insula.com.au/physics/1250/L9.html
Figure 6: https://www2.imperial.ac.uk/earthscienceandengineering/rocklibrary/learntwinning1.php
Figure 8: http://www.enotes.com/topic/Dislocation
Figure 9: http://www.ndtd.org/EducationResources/CommunityCollege/Materials/Structure/linear_defects.htm
Figure 10: http://en.wikipedia.org/wiki/File:Frank-Read_Source.png
Figure 11: Eivind Øvrelid, Casting of mono-multicrystalline silicon for use in solar cells, 18/11-11
Figure 12: Eivind Øvrelid, Casting of mono-multicrystalline silicon for use in solar cells, 18/11-11
Figure 13: http://www.southampton.ac.uk/~engmats/xtal/deformation/control.htm
Figure 14: Eivind Øvrelid, Casting of mono-multicrystalline silicon for use in solar cells, 18/11-11
Figure 15: http://ecee.colorado.edu/~bart/book/book/chapter2/ch2_8.htm
Figure 16: Gaute Stokkan, Dislocations in multicrystalline silicon, November 1st 2011
Figure 18: http://www.oil-analysis.org/ftir_testing.html
Figure 21: http://www.helmholtzberlin.de/forschung/funkma/werkstoffe/methoden/xrd_en.html
Figure 36: *Y.*T. Zhu et al Deformation twinning in nanocrystalline materials

6.2 Text references

[1] European Commision, *Astrategic research agenda for photovoltic solar energy technology*, 2007, ISBN 978-92-79-05523-2

[2]A.G. Ulyashin, *Ge composition dependence of minority carrier lifetime in monocrystalline alloys of Si_xGe_{1-x}*, Material Science in semiconductor processing, number 9, 2006, pages 772-776

[3] Gianmaria Minozzi, *Structural properties of Ge and Hf doped multicrystalline silicon*, master thesis atNorwegian university of science and technology, 2010

[4] M.P. Bellman et al, *The impact of germanium doping on the dislocation distribution in directional solidified mc-Silicon*, Journal of crystal growth, 2011

[5] D. Yang et al, *Germanium-doped crystalline silicon: A new substrate for photovoltaic application*, Journal of crystal growt, 2011

[6] http://www.nobelprize.org/nobel_prizes/physics/laureates/1946/

[7] Flemmings, M.C., *Solidification Processing*, 1974, McGraw-Hill, Inc,. p3

[8] Niklas Letho, *Dislocations in Silicon*, Doctoral thesis Luleå university, page 8 ,1998

[9] Peter Atkins, *Physical chemistry*, 2004, page 568

[10] K. Fuijiwara et al, *In situ observations of crystal growth behavior of silicon melt, Journal of Crystal Growth 243 (2002) 275-282*

[11] O`Mara et al, *Handbook of Semiconductor Silicon Technology*, page 102 ISBN0815512376, 1990

[12] D. Hull, *Introduction to dislocations fourth addition*, page 8, 2001

[13] Charles Kittel, *Introduction to Solid State physics*, page 624, ISBN 978-0-471-41526-8, 2004

[14] Charles Kittel, *Introduction to Solid State physics*, page 607, ISBN 978-0-471-41526-8, 2004

[15] National Renewable Energy Laboratory (USA), www.nrel.gov

[16] Joel I. Gersten et al, *The physics and chemistry of materials*, page 347, ISBN: 9780471057949, 2001

[17] Gaute Stokkan, *Dislocations in multicrystalline silicon*, Lecture notes at NTNU, November 1st 2011

[18] Joel I. Gersten et al, *The physics and chemistry of materials*, page 111

[19] http://www.tf.uni-kiel.de/matwis/amat/def_en/kap_5/backbone/r5_1_1.html

[20] M.P. Bellman et al, *The impact of germanium doping on the dislocation distribution in directional solidified mc-Silicon*, Journal of crystal growth, 2011

[21] Charles Kittel, *Introduction to Solid State physics*, page 601-612, ISBN 978-0-471-41526-8, 2004

[22] D. Hull, *Introduction to dislocations fourth addition*, page 20, 2001

[23] Niklas Letho, *Dislocations in Silicon*, Doctoral thesis Luleå university, page 32-36 ,1998

[24] Eivind Øvrelid, *Casting of mono-multicrystalline silicon for use in solar cells*, Lecture notes at NTNU, 2011

[25] Martin Bellman, Ph.D., Researcher Sintef, Trondheim

[26] O`Mara et al, *Handbook of Semiconductor Silicon Technology*, page 452-462, ISBN0815512376, 1990

[27] S.M. Hu, *Precipitation of oxygen in Silicon: Some phenomena and nucleation model*, Journal of applied physics, 1981, page 3976

[28] J.M. Hwang et al, *Recombination properties of oxygen precipitated silicon*, Journal of applied physics, 1986, page 2476

[29] S.M. Hu, *Precipitation of oxygen in Silicon: Some phenomena and nucleation model*, Journal of applied physics, 1981, page 3975

[30] William C. O`Mara, *Handbook of semiconductor technology* page 527-533, ISBN0815512376, 1990

[31] John Ransford Davis, Jr et al, *Impurities in Silicon solar cells*, IEEE Transctions on electron devices, vol ED-27, NO.4 , april 1980 , pages 677-687

[32] Eivind Øvrelid, *Casting of mono-multicrystalline silicon for use in solar cells*, Lecture notes at NTNU, 2011

[33] William C. O`*Mara Handbook of semiconductor technology page* 97, ISBN0815512376, 1990

[34] Donald R. Askeland, The Science and Engineering of Materials page 256

[35] Dr. M.A. Hopcroft, The youngs Modulus of Silicon

[36] http://www.ioffe.ru/SVA/NSM/Semicond/Ge (On of Russia's largest institute for Science and technology)

[37] R.E. Smallman et al, *Physics Metallurgy and advanced materials, seventh edition*, page 316

[38] Gaute Stokkan, *Characterisation of Multicrystalline Silicon Solar cells*, pages 9-12, Doctoral thesis at NTNU 2004

[39] John Ransford Davis, Jr et al, *Impurities in Silicon solar cells*, IEEE Transactions on electron devices, vol ED-27, NO.4 , april 1980 , pages 682

[40] Gaute Stokkan, *Dislocations in multicrystalline silicon*, Lecture note at NTNU, November 1st 2011

[41] William C. O`Mara Handbook of semiconductor page 99-121 ISBN0815512376, 1990

[42] Gaute Stokkan et al *Characterisation Techniques for Silicon Solar cells*, page 61

[43] User manual for Nicolet 6700 FTIR

[44] Gaute Stokkan et al *Characterisation Techniques for Silicon Solar cells*, page 51, NTNU, 2012

[45] Gaute Stokkan et al *Characterisation Techniques for Silicon Solar cells*, page 118 NTNU, 2012

[46] Gaute Stokkan et al *Characterisation Techniques for Silicon Solar cells*, page 100 NTNU, 2012

[47] Gaute Stokkan et al *Characterisation Techniques for Silicon Solar cells*, page 91 NTNU, 2012

[48] Gaute Stokkan et al *Characterisation Techniques for Silicon Solar cells*, page 141 NTNU, 2012

[49] Joel I. Gersten et al, *The physics and chemistry of materials*, page 347, ISBN0471057940, 9780471057949, 2001

[50] David B. Williams et al, *Transmission electron microscopy*, *Diffraction*, page 249, 1996

51 M. Hirose et al, *Ultra-Thin gate oxide growth on hydrogen-terminated silicon surface*, page 6, Microelectronic engineering 22 (1993) 3.10

[52] J.M. Hwang, *Recombination properties of oxygen precipitated silicon*, Journal of applied physics, Volume 59, 1986

[53] M. Porrini et al, *The effect of oxide precipitates on minority carrier lifetime in p-type silicon containing oxygen precipitates: influence of injection level and precipitate size/density*, pages 244-249, Materials Science and Engineering B73, 2000

[54] Jasprit Singh, Semiconductor device an introduction, Pages 476-478, 1994

[55] H.J Moller, *Oxygen and Carbon precipitation in Multi crystalline solar cells*, Institute fo Experimental Physics, Technical University Bergakademi Freiberg, 1998

[56] N.E. Posthuma, *Development of Stand-alone Germanium solar cells for application in space using spin in diffusants*, 3rd wolrd conference on photovoltaic energy conversion, May 11-18, 2003 Osaka, Japan

[57] Streetman, Ben G.; Sanjay Banerjee (2000). *Solid State electronic Devices* (5th ed.). New Jersey: Prentice Hall. p. 524. ISBN 0-13-025538-6.

[58] Takayuki Akaogi, *Local lattice parameter determination of a silicon (001) layer grown on a sapphire (1Ī02) substrate using convergent-beam electron diffraction*,Journal of electron microscope, 2006

[59] Germanium-doped crystalline silicon: *A new substrate for photovaltaic applications*" by Daren Yang et al